Loss-of-function mutation in IKZF2 leads to immunodeficiency with dysregulated germinal center reactions and reduction of MAIT cells

Hetemäki, Iivo

2021-11-26

Hetemäki , I , Kaustio , M , Kinnunen , M , Heikkilä , N , Keskitalo , S , Nowlan , K , Miettinen , S , Sarkkinen , J , Glumoff , V , Andersson , N , Kettunen , K , Vanhanen , R , Nurmi , K , Eklund , K K , Dunkel , J , Mäyränpää , M I , Schlums , H , Arstila , T P , Kisand , K , Bryceson , Y , Peterson , P , Otava , U , Syrjänen , J , Saarela , J , Varjosalo , M & Kekäläinen , E 2021 , ' Loss-of-function mutation in IKZF2 leads to immunodeficiency with dysregulated germinal center reactions and reduction of MAIT cells ' , Science immunology , vol. 6 , no. 65 , eabe3454 . https://doi.org/10.1126/sciimmunol.abe3454

http://hdl.handle.net/10138/352291
https://doi.org/10.1126/sciimmunol.abe3454

Title:

Loss-of-function mutation in *IKZF2* leads to immunodeficiency with dysregulated germinal center reactions and reduction of MAIT cells

One sentence summary:

Truncating variant of HELIOS causes immunodeficiency with signs of immune overactivation.

Authors:

Iivo Hetemäki[1], Meri Kaustio[2]*, Matias Kinnunen[3]*, Nelli Heikkilä[1], Salla Keskitalo[3], Kirsten Nowlan[1], Simo Miettinen[1], Joona Sarkkinen[1], Virpi Glumoff[4], Noora Andersson[5], Kaisa Kettunen[2,6], Reetta Vanhanen[1], Katariina Nurmi[1], Kari K Eklund[1,7,8], Johannes Dunkel[5], Mikko I. Mäyränpää[5], Heinrich Schlums[9], T. Petteri Arstila[1], Kai Kisand[10], Yenan T. Bryceson[9,11], Pärt Peterson[10], Ulla Otava[12], Jaana Syrjänen[12], Janna Saarela[2, 6, 13,14,§], Markku Varjosalo[3,§], Eliisa Kekäläinen[1]

* § These authors contributed equally to this work.

Affiliations:

1) Translational Immunology Research Program, University of Helsinki and Helsinki University Hospital, Helsinki, Finland

2) Institute for Molecular Medicine Finland (FIMM), HiLIFE, University of Helsinki, Helsinki, Finland

3) Institute of Biotechnology, HiLIFE Helsinki Institute of Life Science, University of Helsinki, Helsinki, Finland

4) Research unit of Biomedicine, University of Oulu, Oulu Finland

5) Department of Pathology, University of Helsinki and Helsinki University Hospital, Helsinki, Finland

6) Department of Clinical Genetics and HUSLAB Laboratory of Genetics, Helsinki University Hospital, Helsinki, Finland

7) Department of Rheumatology, University of Helsinki and Helsinki University Hospital, Helsinki, Finland

8) Orton Orthopaedic Hospital of the Orton Foundation, Helsinki, Finland

9) Center for Hematology and Regenerative Medicine, Department of Medicine, Karolinska Institutet, Stockholm, Sweden.

10) Institute of Biomedicine and Translational Medicine, University of Tartu, Tartu, Estonia

11) Broegelmann Research Laboratory, Department of Clinical Sciences, University of Bergen, Bergen, Norway.

12) Infectious Disease Unit, Department of Internal Madicine, Tampere University Hospital, Tampere, Finland

13) Centre for Molecular Medicine Norway (NCMM), University of Oslo, Oslo, Norway

14) Department of Medical Genetics, Oslo University Hospital, Oslo, Norway

Corresponding Author:

Eliisa Kekäläinen

e-mail: eliisa.kekalainen@helsinki.fi

telephone: +358 50 472 2580

Abstract:

The IKAROS family transcription factors regulate lymphocyte development. Loss-of-function variants in *IKZF1* cause primary immunodeficiency, but Ikaros family member *IKZF2* and *IKZF3* have not been associated with immunodeficiency yet. Here, we describe a pedigree with a heterozygous truncating variant in *IKZF2*, encoding the translational activator and repressor Helios which is highly expressed in regulatory T cells and effector T cells, particularly of the $CD8^+$ T cell lineage. Protein-protein interaction analysis revealed that the variant abolished Helios dimerizations as well as binding to members of the Mi-2/NuRD chromatin remodeling complex. Patients carrying the *IKZF2* variant presented with a combined immunodeficiency phenotype characterized by recurrent upper respiratory infections, thrush and mucosal ulcers, as well as chronic lymphadenopathy. With extensive immunophenotyping, functional assays, and transcriptional analysis we show that reduced Helios expression was associated with chronic T cell activation and increased production of pro-inflammatory cytokines both in effector and regulatory T cells. Lymph node histology from patients indicated dysregulated germinal center reactions. Moreover, affected individuals displayed profoundly reduced circulating MAIT cell numbers. In summary, we show that this novel loss-of-function variant in Helios leads to an immunodeficiency with signs of immune overactivation.

Main Text:

Introduction

The *IKZF2* gene encodes for the zinc-finger protein Helios that can act both as an activator and repressor of transcription. Helios is a member of the Ikaros family of transcription factors, which all share the same structure of two Krüppel-like zinc-finger domains. The N-terminal domain of the protein is required for DNA binding and the C-terminal domain mediates homo- as well as hetero- dimerization with other Ikaros family members, Ikaros and Aiolos(*1*). Ikaros family members have a wide role in the development and function of the immune system. They appear to function through orchestrating chromatin remodeling, in which their interactions with the nucleosome remodeling and histone deacetylase (NuRD) complex, one of the major transcriptional corepressor complexes in mammalian cells, are essential(*2–4*). Both Ikaros and Helios are proto-oncogenes for hematological malignancies - Ikaros in acute lymphoblastic leukemia and Helios in T cell leukemias and acute myeloid leukemia(*4–6*). Mutations in *IKZF1* gene encoding Ikaros have been shown to result in immunodeficiency with variable clinical phenotype depending on the mutation site(*7–9*).

Helios expression is mostly limited to the T cell lineage but young *Ikzf2* knockout mice show no clear immunological phenotype even though a large fraction of homozygous pups perishes for unknown reasons before weaning(*10*). Older *Ikzf2*$^{-/-}$ mice develop an autoimmune phenotype characterized by autoantibodies and dysregulated germinal center reactions(*11*, *12*). Helios is highly expressed in both murine and human T regulatory cells (Tregs) and therefore most studies have focused on its role in peripheral immune tolerance. Helios stabilizes the non-inflammatory phenotype of Tregs, possibly via STAT-5 mediated signaling and prevents IL-2 production in Tregs by epigenetic silencing(*13*), (*14*). In selective knock-out models and

human memory Tregs, Helios-negative Tregs produce more proinflammatory cytokines than their Helios-expressing counterparts(*15*, *16*). However, the suppressive capacity of Tregs is not severely impaired in Helios$^{-/-}$ mice(*12*).

In addition to the constitutively high expression of Helios in Tregs, the expression is also induced after TCR-mediated activation in both Tregs and effector T cells(*17*, *18*). Other factors controlling the expression are unknown, but involvement of NF-κB transcription factor has been suggested(*19*). Studies on T cell exhaustion with LCMV murine infection model identified Helios as one of the most important transcription factors differentiating exhausted virus specific T cells from naive and memory cells(*20*, *21*). It is thus evident that Helios has a significant role in regulating effector T cell activity during immune responses.

Thus far, no germline *IKZF2* variants have been described in humans with a primary immunodeficiency disease (PID). Here we describe a heterozygous *IKZF2* loss-of-function variant in a single family, causing an immunodeficiency with increased immune activation and profound reduction of Mucosal associated invariant T (MAIT) cells. Affected patients have lymphadenopathy with dysregulated germinal centers and aberrations in antibody production reminiscent of the Helios knock-out mouse phenotype. Our results emphasize the importance of the Helios' protein binding domains in mediating its functions in both effector and regulatory T cells.

Results

A novel *IKZF2* variant associated with symptoms of immunodeficiency and immune dysregulation

The index patient (patient 1), a 39 years old female, was referred to our immunodeficiency clinic due to chronic vulvovaginal *Candida albicans* infection, recurrent vulvar and oral mucosal aphtae, chronic lymphadenopathy, and recurrent upper respiratory infections (Table 1). In initial examinations she was diagnosed with hypogammaglobulinemia and is now receiving immunoglobulin replacement therapy. Her father (patient 2), aged 63 years, has suffered from recurrent pneumonias, lichen planus, and oral thrush. He was diagnosed with Hodgkin's lymphoma at the age of 35 and also had chronic lymphadenopathy without lymphoma relapse. More detailed case reports are supplied in the Supplemental clinical data.

We performed whole exome sequencing (WES) for patients 1 and 2 but found no known PID-causing variants. Analysis of WES data filtered for rare variants shared by both patients (Table S1) identified a previously unreported heterozygous variant in *IKZF2* (chr2:213886829 G>T, NM_016260: c.C600A, p.Y200X) that introduces a premature stop-codon in the sequence coding for the fourth DNA-binding zinc-finger of Helios (Figure 1A). Targeted capillary sequencing validated the variant in the two patients and found all other tested relatives homozygous for the reference allele. The combined annotation-dependent depletion (CADD) score for this variant was 38, which is well above the mutation significance cutoff of 3.313 for *IKZF2* (Kircher et al 2014; Itan et al 2016). The position of this novel variant is highly evolutionary conserved (conservation score of 5.8, calculated using GERP++(*22*)) further supporting that the variant is damaging. Targeted capillary sequencing of the patient cDNA indicated that the transcript containing the premature stop codon is not eliminated by the nonsense mediated RNA decay and may produce a truncated protein product (Fig S1A). Based on these observations and previously reported functions of Helios in lymphocytes, we

considered the *IKZF2* c.C600A, p.Y200X (here on p.Y200X for short) variant the most plausible candidate for further studies.

We evaluated the expression of Helios in patients and healthy controls performing immunoblot from both unstimulated and stimulated peripheral blood mononuclear cells (PBMC). The patients showed a marked reduction in total Helios protein already in unstimulated cells but we could not detect the p.Y200X truncated protein (Fig 1B, Fig S1B-C). Also with flow cytometry, Helios mean fluorescent intensity was considerably lower in patients in both $CD4^+$ and $CD8^+$ T cells compared with both healthy controls and two unaffected relatives (index patient's sister 38 yrs and cousin 44 yrs, both females) (Figure 1C, Fig S1E).

Since Ikaros family members are known to form functional heterodimers between each other(*3*), we also quantified the expression of Aiolos and Ikaros in patients. Mean expression of Aiolos was higher in patients in total $CD4^+$ helper T cells when compared with healthy controls (Fig 1D). However, this difference was explained by an expansion of fully mature T cells in expense of $Aiolos^{low}$ naïve cells in patients (Figure 2A). Mature $CD4^+$ T cells expressed higher level of Aiolos also in healthy controls and the expression level in different $CD4^+$ maturation stages was comparable between patients and controls (Fig S1G-I). No differences in Ikaros expression were detected (Figure 1D, Fig S1F). In summary, the novel *IKZF2* variant resulted in diminished Helios expression in affected individuals with no differences in expression levels of other Ikaros family members.

Truncating variant abolishes Helios' interactions with Mi-2/NuRD complex components

Since the variant's premature stop-codon prevented the translation from the second zinc-finger domain onwards, we reasoned that it most likely affects the variant's protein-protein interactions. In order to determine possible changes in interactions we performed biotin proximity ligation (BioID,(*23*)) in generated stable cell lines, expressing Helios constructs with MAC tag(*24*). The variant p.Y200X lost protein-protein interaction with 48 proteins compared

with wild-type Helios. Furthermore, interaction with 187 protein partners was significantly reduced compared to the wild-type Helios (Fig 1E and Table S2). Ikaros family members have a central role as part of the Mi-2/NuRD complex(*25*). The truncated Helios variant had reduced or lost interaction with 12 proteins involved in the Mi-2/NuRD complex, including the essential core proteins CHD3 and MTA1(*26*).

Since Ikaros family members heterodimerize strongly with each other, we tested if the variant p.Y200X affected Helios' dimerization with Ikaros and Aiolos. In a co-immunoprecipitation assay the variant's dimerization with both Aiolos and Ikaros was markedly impaired compared to the wild-type Helios (Fig 1F).

We used the ClueGo clustering tool(*27*) to identify the biological processes that were affected by variant's lost protein-protein interactions. The proteins with altered interaction with the truncated Helios had functions predominantly linked to DNA modulation and transcription (ClueGO_MF, Table S2), and transcriptional repressors (ClueGO_BP, Fig 1G, Table S2). The interactome analysis thus confirmed that the patient-derived *IKZF2* truncating variant impaired key Helios protein-protein interactions.

Increased T cell differentiation and augmented proinflammatory proteins in patients with the *IKZF2* p.Y200X variant

Immunophenotyping of T lymphocytes in the patients showed a decreased proportion of naïve $CD8^+$ T cells with concomitant expansion of memory subsets. Especially the proportion of $CD45RA^+CCR7^-$ T effector memory RA^+ (TEMRA) cells was higher in patients (Table 1). In $CD4^+$ cells similar, though less pronounced, bias towards memory phenotype was observed. Patients also had an increased number of activated $CD38^+HLA\text{-}DR^+$ cells *ex vivo* in both $CD4^+$ and $CD8^+$ T cell subsets (Table 1). In a more detailed flow cytometry immunophenotyping we could detect a skewing from naive T cells to effector memory - like phenotype that is also associated with T cell senescence (Fig 2A-B, Fig S2A).

In order to decipher the origin of the chronic activation in patients' T cells, we used a custom gene panel (50 genes linked to immune signaling and inflammasome activation) with Nanostring nCounter(*28*) to screen for gene expression profiles in the patients' PBMCs *ex vivo*. Both patients had a marked upregulation of genes related to both type 1 and type 2 interferon, NF-κB, and JAK-STAT signaling (Fig 2C). Also a number of genes associated with inflammasome signaling were upregulated.

Cytotoxic $CD8^+$ T cells had the highest Helios expression of effector T cell populations analyzed (Fig S2C-D) so we decided to do RNA sequencing (RNASeq) on $CD8^+$ T cells from patients and age and sex matched healthy controls. In differential expression analysis several immunoregulatory and functional genes had altered expression in patients, such as upregulation of SMAD7 and downregulation of CD101 (Table S3). Pathway analysis showed that IFN-γ and IL-1β downstream signaling pathways were markedly upregulated in patients (z-score 2.304, p=1x10-7 and Z-score 2.543 and P=6x10^-7 respectively, Table S4).

RNASeq showed that expression of genes S100A8 and S100A9 were upregulated in patients' CD8 positive T cells *ex vivo* when compared with age and sex matched healthy controls (Fig 2D, Table S3). These genes code for a heterodimer called calprotectin that is a strong proinflammatory alarmin molecule(*29*). To confirm the RNASeq result, we measured the total calprotectin level from patients´ sera. Patient 1 had 6.58 mg/l and patient 2 11.49 mg/l of total calprotectin in their serum, i.e. 1.2 and 2.1 times higher than the upper limit of reference values generated from healthy donors(*30*). The non-affected relatives had normal levels of calprotectin (1.95 and 3.72 mg/l).

Calprotectin can activate inflammasome through TLR4 and induce IL-1β production from target cells (*31*). In RNASeq and NanoString several genes related to inflammasome activation were upregulated in patients. As a sign of inflammasome activation, IL-1β serum concentrations were elevated in both patients: 1.95 pg/ml for patient 1 and 0.59 pg/ml for

patient 2. All healthy controls were below the detection level of 0.31 pg/ml (n=21). Analysis of culture media of unstimulated PBMCs revealed increased spontaneous secretion of IL-1β for patients, although less pronounced for patient 2 (Fig 2E). However, no clear differences in inflammasome activation or cellular death were detected in comparison with healthy controls when patients' PBMCs were activated with LPS and combination of LPS and ATP (Fig S3).

These data indicate that the patients with the heterozygous p.Y200X variant, display a proinflammatory transcriptional signature both in their PBMCs and cytotoxic T cells. The increased proinflammatory milieu was also reflected by elevated serum levels of potent proinflammatory proteins.

Increased IFNγ and IL-2 signaling in T cells from patients with the *IKZF2* p.Y200X variant

Helios is upregulated in response to TCR activation and currently there are no other known signaling pathways that control Helios' expression(*17*). With an anti-CD3/CD28 co-stimulation on PBMCs *in vitro*, healthy controls showed a marked upregulation of Helios, especially in $CD8^+$ T cells. Our patients, however, failed to upregulate Helios (Fig 3A, Fig S4A&B).

Next we performed RNASeq on purified T cells from patients and age-sex matched healthy controls after 24 hr stimulation with anti-CD3/CD28 antibodies. Whereas only 10 genes were differentially expressed in the unactivated state (Fig S4D & Table S3), 103 genes showed differential expression after anti-CD3/CD28 stimulation including 16 downregulated and 87 upregulated genes (Fig S4E & Table S3). Analysis of sample pairs from the same individuals prior and after anti-CD3/CD28 stimulation also allowed us to compare transcriptional changes between groups in response to activation. Pearson's correlation coefficient between patients and controls was 0.8, showing that by-and-large both groups exhibit similar up- and downregulation of gene expression in response to anti-CD3/CD28

stimulation (Fig 3B) and in patients most of the differentially upregulated genes either retain higher expression or are upregulated more after anti-CD3/CD28 stimulation compared to controls.

In pathway analysis of differentially expressed genes after anti-CD3/CD28 activation both IFN-γ and IL-2 downstream signaling was upregulated in patients (z-score 2,129, p-value 8x10^-10 and z-score 3,875, p-value 8x10^-13, respectively; Table S4). Also the T cell exhaustion transcriptional signature (z-score 0,813, p-value 1x10^-4) and NF-ϰB signaling pathway (z-score 1,342, p-value 0,005) were upregulated compared with healthy controls. When we cross-analyzed the protein partners whose interaction with the variant Helios was affected, we could detect changes in downstream signaling of several of Helios' protein partners (Table S4). Taken together, the transcriptional landscape after anti-CD3/CD28 stimulation in patients with the p.Y200X variant of *IKZF2* compared with healthy controls indicated immune dysregulation of several major immune activation pathways.

Both Nanostring analysis on PBMCs and RNASeq T cells *ex vivo* and after stimulation suggested increased IFNγ signaling. Analysis of chemokine receptor expression on memory T helper cells *ex vivo* also indicated a strong Th1 polarization as indicated by higher fraction of CCR6-CXCR3+ cells in patients (Fig S4G)(*32*). Another important pro-inflammatory cytokine controlled by Helios is IL-2(*13*), (*14*) so we analyzed the IFN-γ and IL-2 production in T cells after anti-CD3/CD28 stimulation. Increased proportion of IFN-γ - and IL-2 - producing cells was observed in patients in response to anti-CD3/CD28 stimulation (Fig 3C&D, Fig S5). IL-2 receptor alpha chain (CD25) expression levels were lower *ex vivo* in patients compared to controls (Fig 3E, Fig S4A). Low CD25 could result from downregulation of the IL-2 receptor in response to higher baseline level of IL-2. We also measured the soluble CD25 from patients' sera and it was within reference values (Suppl Clinical data). The kinetics of activation marker expression after anti-CD3/CD28 stimulation on both CD4 and CD8 effector T cells were

comparable between patients and healthy controls indicating that reduced Helios expression does not affect the overall expression of activation markers on T cells (Fig 3F&G, Fig S4). One patient had significantly reduced proliferative response of both $CD4^+$ and $CD8^+$ T cells to anti-CD3/CD28 stimulation as measured by both CFSE assay and failed upregulation of Ki67 (Fig 3F&G, Fig S4H).

To summarize, reduced expression of Helios in effector T cells is associated with increased production and downstream signaling of proinflammatory cytokines in response to TCR stimulation.

Patients with the *IKZF2* p.Y200X variant have an increased proportion of T regulatory cells with a proinflammatory phenotype

Helios expression is high in Tregs and it stabilizes Treg suppressive function in mice(*11*). In our patients, the proportion of circulating naive and activated Tregs was lower than in healthy controls or unaffected relatives (Fig 4A, Fig S6A). More detailed characterization of Tregs revealed a shift from naive Tregs to more mature phenotype in patients as in T cells in general. Proportion of recent thymic emigrant Tregs was also lower in patients (Fig 4B, Fig S6B). We could not, however, detect changes in the suppressive function of Tregs with *in vitro* suppression assay (Fig 4C). Patients' Tregs had higher expression level of immunosuppressive protein receptor CTLA-4 and suppressive adenosine producing ectonucleotidase CD39 (Fig 4D, Fig S6A-C).

In vitro Treg suppression assays have several limitations and do not reflect all functional aspects of Tregs so we continued to do a FoxP3 TSDR methylation and transcriptome analysis of Tregs. We sorted $CD127^-CD25^{hi}$ T cells from patients and age and sex matched healthy controls (Fig S5C). We analysed the FoxP3-TSDR methylation status from sorted Treg cells from P1 and the result indicated comparably high demethylation of the

promoter region as in healthy controls (Fig S6D). In general, the changes in Treg transcriptome were less pronounced than in effector T cells and analysis might have been affected by the low number of Treg cells obtained from patients. As in effector T cells the IFN-γ and NF-κB signaling were higher in patients (z-score 2,271, p-value 9x10^-9, and z-score 1,623, p-value 2x10^-4, respectively, Table S4). These most likely reflect the overall proinflammatory milieu in the patients. However, some Treg-specific changes could be seen. For example the paraprotein convertase Furin expression was higher in patient Tregs (Fig 4F). Furin has been reported to be important for the suppressive capacity of Tregs and it is upregulated in the activated Tregs(*33*, *34*). Together, Furin, CD39, and CTLA-4 upregulation indicate that patients' Tregs were more activated than in healthy controls (Fig S6C).

Helios-deficiency has been reported to lead to proinflammatory cytokine production in murine Tregs (*11*)(*14*). After *in vitro* CD3-CD28 co-stimulation of freshly isolated T cells the patients' Tregs had a higher proportion of IL-2 producing Treg cells but there was no clear difference for IFN-γ production (Fig 4E, Fig S5). Since diminished IL-2-STAT5 signaling has been linked to Treg instability in Helios$^{-/-}$ mice(*11*) we measured STAT5 phosphorylation in response to IL-2 stimulation. No differences were observed (Fig S6F). These data indicate that Tregs in patients with *IKZF2* p.Y200X variant are skewed towards a more activated and mature phenotype.

Finally, we wanted to study whether the increased IFN-γ and IL-2 signaling and production in patient effector cells would be secondary to aberrant Helios signaling in Tregs or a true effector cell - intrinsic effect. We knocked down Helios in healthy donor T cells using commercially available Helios silencing RNA (siRNA, Fig S7). After Helios-knockdown, *in vitro* activated Tregs more often produced IL-2 and IFN-γ (Fig. 4G, Fig S7A-B and D). When we analyzed the effector CD4 cells, the increase of proinflammatory cytokine producing cells was more pronounced (Fig. 4H, Fig S7D). Helios-knockdown also resulted in lower CD25

expression (Fig. 4I). Due to the short stimulation, the increased production of proinflammatory cytokines cannot only result from defective Treg function but reflects an effector cell intrinsic effect of the lost Helios suppression.

Dysregulated germinal center reactions and aberrant antibody production in patients with the *IKZF2* p. Y200X variant

Both patients' clinical presentation with recurrent upper and lower respiratory infections suggested common variable immunodeficiency - like B cell pathology. Clinical immunophenotype of the B cells revealed an increased proportion of transitional B cells in both patients. Patient 1 also had a higher number of activated B cells, but a decreased amount of switched memory B cells and plasmablasts in line with hypogammaglobulinemia. Since Helios expression in B cells is low (Fig S1G and S2C&D) we reasoned the B cell defect could result from impaired T cell help to B cells. Supporting this assumption, Helios knockout mice have defective regulatory follicular T cells (Tfr) with accumulation of Tfh cells to the lymph node and aberrant germinal center formation(*12*). Moreover, in humans Helios has been suggested to have a role in the Tfh cell differentiation *in vitro(19)*. To evaluate the role of Helios in human Tfh and Tfr cells we measured Helios expression in these subsets isolated from fresh lymph node samples obtained from organ donors. Helios expression in Tfr cells was comparable to non-follicular Tregs (Fig 5A&B, Fig S8A). In Tfh cells Helios expression was lower than in Tfr but higher when compared to non-follicular effector T cells (Fig 5A&B).

In peripheral blood, T cells positive for the homing marker CXCR5 form a population enriched for circulating Tfh cells. Their number was markedly lower in patients' peripheral blood (Fig 5C, Fig S8B) and we could not reliably detect circulating $CD4^+FOXP3^+CXCR5^+$ regulatory follicular T cells from patients while in controls they accounted for 0,23 (+/- 0,11) % of $CD4^+$ cells.

293 Since Tfh cells carry out their effector functions in lymph nodes we performed
294 immunohistochemical analyses on archival resected lymph nodes from both patients. The
295 lymph nodes were removed due to persistent lymphadenopathy and were non-malignant.
296 Pathologic-anatomic diagnosis on both was follicular hyperplasia, a common unspecific
297 finding in a variety of diseases, including autoimmunity. In a more detailed
298 immunohistochemical analysis both patients had increased $CD3^+$ cellularity in the perifollicular
299 region. These cells expressed high levels of Bcl6 and PD1 so they most likely represent an
300 accumulation of Tfh cells in the perifollicular region around the germinal centers (Fig 5D). We
301 also detected an increased proliferative activity as indicated by the high Ki67 labeling index.
302 The lack of circulating Tfh cells and accumulation of Tfh-like cells in the light zones
303 of the lymph nodes suggest a dysregulated germinal center reaction that often leads to
304 production of autoantibodies. Both patients were at the time of clinical examination negative
305 for anti-nuclear autoantibodies and anti-thyroid autoantibodies even though both had
306 hypothyroidism (Suppl Clinical Data). We next measured neutralizing autoantibodies against
307 cytokines that have been reported in a number of immune dysregulatory
308 conditions(*35*). Patient 2 had high titers of antibodies against multiple cytokines, especially
309 type 1 interferons (Fig 5E). This anti-cytokine autoantibody profile was reminiscent of what is
310 commonly seen in APECED patients(*36*) which is a syndrome of severe immune
311 dysregulation. Patient 1 had hypogammaglobulinemia and also her pneumococcal vaccine
312 responses were impaired (Table 1 & Suppl Clinical Data) so autoantibody measurements were
313 unreliable. Anti-cytokine antibody titers against few cytokines were slightly higher in patient
314 1 sera compared to controls but not in the magnitude exhibited by patient 2 (Fig S8B).
315 We can conclude that patients with heterozygous p.Y200X variant in *IKZF2* had
316 abnormal antibody findings - hypogammaglobulinemia and anti-cytokine autoantibodies -
317 together with signs of T follicular helper cell dysregulation in the lymph nodes.

MAIT cells are reduced in circulation and in gut epithelium of patients with the *IKZF2* p.Y200X variant

Innate lymphoid cells including Natural Killer cells (NK) have been reported to express HELIOS(*37*) but NK cell immunophenotyping from the patients did not show any significant perturbations in NK cell subpopulations (Fig S9). MAIT cells are innate like T cell subset contributing to bacterial defense on mucosal surfaces and have a high expression level of Helios(*38*). MAITs also recognize fungal metabolites *in vitro* but their role in fungal defence *in vivo* is unclear(*38*). Since both patients had mucosal *Candida albicans* infections and recurrent bacterial infections, we next decided to analyze their MAITs. In comparison to healthy controls and unaffected relatives, the number of Vα7.2^{+}CD161^{hi} T cells in circulation was markedly reduced in patients (Fig 6A-B). The small number of Vα7.2^{+}CD161^{hi} T cells detected in patients also had lower Helios expression than healthy controls (Fig 6C). MR1 tetramer loaded with 5-(2-oxopropylideneamino)-6-D-ribitylaminouracil (5-OP-RU) is specific for the invariant TCR found in majority of MAITs(*39*). Only 84% of patients' Vα7.2^{+}CD161^{hi} cells were positive for 5-OP-RU loaded MR1 tetramer compared to 97% in the controls (Fig 6D, Fig S10A). Also, the proportion of CD8^{+}CD4^{-} MAITs, proposed to represent a more active phenotype(*40*), was lower in patients while the expression of activation and tissue retention marker CD69 was higher in patients' MAITs (Fig 6D, Fig S10A).

Reduced MAIT number in the blood can be caused by their recruitment to sites of inflammation in the periphery as seen in e.g. inflammatory bowel diseases(*41*). Both of our patients had unspecific gastrointestinal complaints but no diagnostic findings were made in the endoscopies. We measured MAITs by flow cytometry from intestinal biopsies taken during clinically indicated esophagogastroduodenoscopy (both patients) and a colonoscopy (patient 1). The proportion of Vα7.2^{+}CD161^{hi} MAIT cells isolated from mucosal biopsies of patients was not higher when compared with samples obtained from organ donors (Fig 6E-F, Fig S10B).

344 Therefore, the low proportion of MAITs in circulation appeared not to be a result of an
345 increased accumulation to the gut mucosal sites.

346 The role of HELIOS expression in MAITs is unknown. MAITs develop in the thymus
347 as a minor population. They expand and acquire effector memory - like phenotype quickly after
348 egressing from the thymus(*42*). We wanted to evaluate at which stage of their development
349 and function MAITs start to express high levels of Helios. We analysed the expression of
350 Helios in developing MAITs isolated from thymic samples (n=4) acquired from children
351 undergoing cardiac surgery. As reported before, the percentage of developing MAITs was low
352 and only 0,025% (+/-0,015%) of thymocytes were positive for the MR1-5-OP-RU-tetramer.
353 The majority of MR1-tetramer positive thymocytes expressed Helios (93,5% +/- 5,6%, Fig
354 S10C&D). Next, we used stimulation with *E. coli* and *C. albicans* on PBMCs(*43*) from healthy
355 donors to measure if Helios is involved in the peripheral activation of MAITs. Unstimulated
356 MAITs were already predominantly Helios positive but both microbial stimulations caused a
357 robust upregulation of Helios in MAITs (Fig 6G). We can therefore conclude that Helios is
358 expressed both during the thymic development of MAITs and their activation in the periphery.

Discussion

Here we describe a novel immunodeficiency with signs of immune dysregulation caused by heterozygous germline loss of function mutation in *IKZF2* coding for the transcription factor Helios. The truncating mutation found in this single pedigree profoundly changed the ability of Helios to interact with proteins of the NuRD complex and other members of the Ikaros family. Affected patients had a reduced level of Helios expression in their peripheral T cells and specific immunophenotypic changes in T cell populations expressing high levels of Helios, especially MAIT cells. The immunophenotype segregated in the pedigree with the carriers of the loss-of-function *IKZF2* variant.

Protein interactome analysis of the truncated protein variant showed that it lost interaction with key components of the NuRD complex, the protein complex in which Ikaros family members are involved in chromatin remodelling(*3*). RNAseq of stimulated primary patient lymphocytes confirmed altered gene expression directly downstream of some of the transcription factors identified with the interactome analysis. For example, downstream signaling for histone acetyltransferase EP300, that we found to interact only with wild type but not with the variant protein, was altered in all three RNAseq conditions (Tables S2&S4). Based on our findings, the interactions with the NuRD complex are essential for Helios' function.

Helios acts mainly as a transcriptional repressor in lymphocytes(*3*, *4*). In accordance with this, we detected increased proinflammatory signaling and production of proinflammatory cytokines and proteins in the carriers of the p.Y200X variant. The chronic overactivation of the immune system is most likely the cause for the patients' activated mature T cell - skewed immunophenotype. Our detailed analysis of patients' immune system concurs with earlier data acquired in murine models, but also offers new insight into the role of Helios in regulating immune responses. Helios represses IL-2 production(*14*). In our patients, we saw enhanced IL-2 production from both effector and regulatory T cells and could replicate that finding with

Helios knockdown in primary T cells. Also the transcriptome analysis of T cells indicated increased IL-2 signaling. Interestingly, patients' cytotoxic T cells produced higher amounts of calprotectin, which is an alarmin molecule responsible for e.g. sterile inflammasome activation. Calprotectin is used in various clinical settings to evaluate subclinical systemic inflammation(*44*). Concomitantly the patients had increased levels of IL-1β cytokine, reflecting the inflammasome activation.

The studies on the role of Helios in controlling immune responses have mainly concentrated around its effects on regulatory T cells. Selective Helios knockdown with the Foxp3 promoter is sufficient to induce autoimmunity in mice(*11*, *12*). On the other hand, in Helios$^{-/-}$ mice suppressive capability of Tregs *in vitro* is intact and their *in vivo* function is only mildly impaired(*12*, *45*). Our patients had only mild autoimmune manifestations. The Treg *in vitro* suppression assay did not indicate any reduction in suppressive capacity but especially when done in a single effector:Treg ratio the limited sensitivity of the assay should be taken into account, as subtle changes in suppressive function might remain undetected. Moreover, patients' Tregs were skewed towards a more mature immunophenotype with high CTLA-4 expression and signs of activation, which could indicate some compensatory mechanisms making up for the reduced Helios expression. Helios has been suggested to stabilize the suppressive phenotype of Tregs(*14*) and a loss of Helios could cause Treg conversion to effector T cells(*15*). Patients' Tregs had a more inflammatory phenotype with increased IL-2 production and lower FoxP3 and Helios expression, which is characteristic of unstable Tregs(*15*, *46*). Selective knockout of Helios from human fetal induced Tregs also resulted in a similar phenotype (*13*). Our results confirm earlier reports that Helios has a limited role in stabilizing human Tregs.

Germline knockdown of Helios or selective knockdown of Helios with Foxp3 promoter increases germinal center formation and accumulation of Tfh and germinal center B cells in

lymph nodes(*12*). In patients' lymph nodes we could see an accumulation of perifollicular T cells that are considered the precursor population for mature Tfh cells. Similar increase of Tfh cells in lymph nodes after immunization was evident in Helios heterozygous mice(*12*). Circulating $PD1^{hi}CXCR5^{+}$ Tfh cells are fully mature memory cells that have exited from the germinal centers(*47*). In our patients, the circulating CXCR5 positive Tfh cells were almost undetectable. It is thus possible that Helios is required for the terminal Tfh differentiation within the germinal center. Another plausible explanation is that Helios is somehow involved in the Tfh egress to circulation.

One other defining feature of our patients was the marked reduction in the number of MAITs in the peripheral blood. This could be a result of increased homing of MAITs to mucosal tissues but analysis of mucosal biopsies from the patients detected only a small fraction of MAITs. Both patients suffered from recurrent mucosal bacterial and *C. albicans* infections complicated with aphtae. We speculate that the loss of MAITs from mucosal surfaces, where they should be a relatively abundant innate effector cell population, could play a role in these clinical symptoms(*48*). Deficiency of Helios could also harm the MAIT development in the thymus or their peripheral activation and expansion. Since the patients had so few MAITs we could only perform experiments on MAIT biology in cells from healthy donors. Based on our findings in the healthy human thymus we can conclude that Helios is highly expressed already in developing MAITs. However, Helios expression was also high in mature effector MAITs and even further upregulated after microbial stimulation. Thus, although our data is inconclusive on at which stage the loss-of-function variant in *IKZF2* could affect the MAIT numbers, our data supports a non-redundant role for Helios in MAITs. An alternative explanation is that the chronic inflammation in patients caused the MAIT cell depletion. MAIT cell numbers have been shown to have an inverse correlation with levels of innate proinflammatory cytokines in various inflammatory conditions(*49*, *50*). The patients

also had excessive IFN-γ responses that might also contribute to mucosal candidiasis as was recently suggested to be the case in patients with APECED (*51*).

Clear limitation of our study is the small number of patients from a single family. This is bound to affect e.g. RNASeq analyses since some of the differences we detected could be caused by other inheritable factors than the *IKZF2* variant. However, our results from these two patients recapitulate the main findings from Helios knock-out mice – IL-2 producing Tregs and dysregulated germinal centers. In addition to Helios' known effects on the immune system, we show that Helios has a previously underappreciated role in the MAIT cell lineage. Further studies are needed to understand what the functional significance of Helios is both in the control of germinal center reactions and MAITs.

Studies on patients with mutations in *IKZF1* encoding Ikaros indicate that the clinical sequela of Ikaros mutation is determined by the mutation site. Heterozygous missense mutations in Ikaros cause CVID-like immunodeficiency with progressive loss of B cells in the circulation with a variable penetrance of the clinical disease(*7*). Dominant negative mutations in Ikaros lead to an early onset combined immunodeficiency phenotype with disturbed T cells effector maturation and dysfunctional monocytes(*8*). Mutations of Ikaros that disrupt the dimerization function at the C-terminal end, as *IKZF2* p.Y200x does for Helios, result in reduced sumoylation and protein stability(*9*). Our data suggests that a similar mechanism might be at play for the *IKZF2* p.Y200X variant. While the variant was translated to RNA (Fig S1A) and the truncated protein was readily produced in a cell line, we were unable to detect the truncated protein from primary patient cells. This could result from decreased protein stability. BioID indicated that interactions of several proteins involved in sumoylation, such as SUMO2, were decreased for the p.Y200X variant compared to wildtype Helios.

Finally, the clinical features of dimerization disruptive *IKZF1* variants include among others hematologic malignancies, B cell lymphopenia, and hypogammaglobinemia, but only

460 mild immunodeficiency (*9*) - a phenotype which is not dissimilar to our small sample of
461 patients. In contrast, Shahin et al. in this same issue show that homozygous missense mutation
462 in Helios leads to combined immunodeficiency with hypofunctional T cells. These variable
463 immunological presentations highlight the complex roles Ikaros family of transcription factors
464 including Helios have as activators and repressors of transcription in T cells and rest of the
465 immune system.
466

Materials and methods

Study design

Two patients with a previously uncharacterized immunodeficiency were identified in immune deficiency clinic. WES identified a heterozygous variant in *IKZF2* that introduces a premature stop-codon and we validated deleterious effects of the variant with protein interaction analyses. We evaluated the impact of the Helios variant with extensive characterization of the patients' immune system including effector T cells, Tregs, follicular T cells, MAITs, B cells, and inflammasome activation from patients' primary samples from both blood and tissue.

Study subjects and samples

The study was conducted according to the principles of the Declaration of Helsinki. The study was approved by the ethics committee of Helsinki University Hospital (138/13/03/00/2013 and HUS/747/2019) and written informed consent was obtained from participants. The control group for blood samples consisted of 25 healthy individuals aged 24-66 (mean 46) years, 14 of them female. In addition samples were acquired from two relatives of the patients without mutation in *IKZF2* gene (index patient's sister 38 yrs and cousin 44 yrs, both females). The number of controls varied among experiments and it is indicated either in the figures or in the text. In experiments containing less than 10 healthy controls the controls were sex and age matched.

Patients' clinical T- and B- cell phenotype, total blood count, immunoglobulin levels, complement activity and anti-tetanus and -diphtheria antibodies were evaluated by clinically validated test in Tampere University Hospital's clinical laboratory Fimlab (Tampere, Finland). Samples from duodenum and colon were acquired from the patients during diagnostic endoscopy. Lymph node samples from patients were archival diagnostic samples. Control tissue samples were obtained from organ donors: duodenum from four individuals (34-69

493 years, 2 female) and colon from one individual (43 years old female), and lymph node samples
494 for characterization of follicular T cells (age 19-41, all male). Samples of the human thymus
495 were obtained from four children undergoing cardiac surgery (aged 15, 18 and 18 days and 15
496 years, 3 female).
497
498 **DNA extraction and sequencing**
499 Genomic DNA was extracted from EDTA blood with the Qiagen FlexiGene DNA kit (Qiagen)
500 or from Oragene OG-575 saliva collection kit with the prepIT-L2P kit (DNA Genotek). For
501 RT-PCR, RNA was extracted with the Qiagen miRNeasy kit (Qiagen) from freshly isolated
502 PBMCs, and reverse transcribed into cDNA using SuperScript™ VILO™ cDNA Synthesis Kit
503 (ThermoFisher). Exome and capillary sequencing were performed at the sequencing core
504 facility of the Institute for Molecular Medicine Finland (FIMM). Exome libraries were
505 generated using the Clinical Research Exome (Agilent Technologies) or the Nextera Flex
506 (Illumina) capture kits, and sequencing was performed with 101 bp read length on the
507 HiSeq1500 or the NovaSeq6000 Sequencing Systems (Illumina), respectively. Read mapping
508 and variant calling were performed with an in-house pipeline. Variant annotation was
509 performed with ANNOVAR(*52*). Variant data was filtered following a dominant inheritance
510 model as described in Table S1. For frequency filtering, we utilized population level variant
511 frequency data from the Genome Aggregation Database (gnomAD)(*53*) and 1000
512 genomes(*54*). Recurrent sequencing artefacts and bad quality variants were excluded based on
513 in-house data and visual inspection of reads on the Integrative Genomics Viewer(*55*).
514 Candidate variants were validated by targeted PCR by DreamTaq Green PCR Master Mix
515 (ThermoFisher) and capillary sequencing on the ABI3730XL DNA Analyzer (Applied
516 Biosystems). All primers used for PCR and capillary sequencing are listed in Table S5.
517
518 **Immunoblot**

519 PBMCs were thawed and either left in media (RPMI+10% FBS+PS+L-glut) overnight, or
520 immediately stimulated with 1 μg/ml anti-CD3 and anti-CD28 (eBioscience/ThermoFisher)
521 and 10 ng/ml IL-2 in 37 C incubator for 3 days, after which culture was continued for 7 d
522 samples in media with IL-2.
523
524 Whole cell protein was extracted by lysis of PBMCs in RIPA-buffer with Pierce protease
525 inhibitor (Thermo Scientific). 4 μg of whole protein extracts were run on 15-well 4-15% Mini-
526 PROTEAN® TGX™ precast protein gels and blotted onto LF-PVDF membranes with the
527 Trans-Blot Turbo Transfer System (Bio-Rad). Blot was probed by anti-Helios and secondary
528 HRP antibodies (Table S5) and detected with ECL reagents (Advansta, Pierce) on the
529 ChemiDoc™ MP Imaging System (Bio-Rad). For loading control, total protein was stained
530 with No-Stain™ Protein Labeling Reagent (Invitrogen). Total protein stain lane intensity was
531 detected and Helios band intensity was normalized to total protein stain using ImageLab 6.0
532 (Bio-Rad).
533
534 **Protein-protein interaction analysis**

535 Biotin proximity ligation assay was done with stable cell lines, generated from Flp-In™ T-
536 REx™ 293, expressing Helios constructs with N-terminal MAC tag ((*24*). Cell line generation,
537 sample preparation and mass spectrometry was done as previously described(*24*), with the
538 exception of using 1% N-dodecyl maltoside instead of 0.5% IGEPAL in the lysis and wash
539 buffers.

540 Peptides with a false discovery rate (FDR) of <0.05, were exported from the peptides detected
541 with mass spectrometry. Identified proteins were compared against the Contaminant repository
542 for affinity purification database(*56*). Only interactions with <20% frequency and 2-fold higher

abundance, compared to the corresponding protein values in the controls database, where classified as high-confidence interactions. The Cytoscape software platform (*57*) was used to visualize the high-confidence protein-protein interactions. ClueGo plugin (*27*) was utilized for clustering of biological processes the identified proteins contributed to.

Co-immunoprecipitation

6*10^5 HEK293 cells were co-transfected with 1 µg of either HA tagged wild type *IKZF2* or C600A *IKZF2* and V5 tagged *IKZF1* or *IKZF3*. 24h after transfection, cells were washed with cold PBS, lysed on ice for 15 min in 1 ml of ice-cold lysis buffer (0.5% IGEPAL, 50mM HEPS, 5mM EDTA, 150mM NaCl, 50mM NaF pH 8.0 supplemented with 1mM DTT, 1mM PMSF, 1,5mM $NaVO_4$, 1x Sigma protease inhibitor cocktail). Lysates were centrifuged 16 000g, +4°C for 15 min to remove insoluble debris. 20 µl of supernatants were taken into fresh tubes with 20 µl 2x laemmli sample buffer and incubated at 95°C for 5 min (lysate sample). 950 µl of supernatants were moved to new tubes with 30 µl of washed anti-HA beads (A2095, Sigma), and incubated 2h on rotation in +4°C. Beads were spinned down and the supernatant was discarded. The beads were washed three times with 1 ml of ice-cold lysis buffer. The immunoprecipitated proteins were eluted with a 2x laemmli sample buffer and incubated at 95°C for 5 min and the beads were spinned down (Co-IP sample).

Co-immunoprecipitation (10 µl) and lysate (5 µl) samples were loaded on precast SDS-PAGE gels (any kD gel with 15 wells, Mini-Protean TGX, Bio-Rad) and transferred onto nitrocellulose membrane (NBA085C001EA, PerkinElmer) with semi-dry transfer (Trans-blot SD semi-dry transfer cell, Bio-Rad). The membranes were blocked with 5% milk – in 0.05% Tween – TBS. Primary antibodies were detected with a secondary antibody coupled to HRP (Table S5). ECL reaction (RPN2232, Amersham) was developed on photographic films (Super RX-N, Fuji X-ray films).

Sample preparation

Blood was drawn into Li-heparin Vacutainer tubes (BD Biosciences), plasma was separated by centrifugation, and PBMCs isolated using Ficoll-Paque (GE Lifesciences) gradient centrifugation. The cells were cryopreserved using CTL-Cryo ABC (CTL) kit. Cryopreserved samples were used unless otherwise stated.

Immune cells from fresh tissues were extracted within a maximum of 6 hours of operation and analyzed subsequently. The duodenal samples were transported in full media on ice, cut in small pieces, rinsed with PBS and incubated in 5 mL of enzyme solution (RPMI containing 15 mM HEPES, 0.25 mg/mL of DNAse I and 0.25 mg/mL of collagenase II) on a magnetic shaker in +37°C water bath for 20-30 min. The tissue digest was filtered with a 100 micron filter and washed first with cold PBS containing 10% FCS or human AB media. Lymphocytes from lymph nodes and thymocytes from thymic resecates were released with mechanical homogenisation. All single cell sample solutions were washed 2 times with a staining buffer (PBS containing 2% FCS and 2 mM EDTA) before use in downstream applications.

Flow cytometry

For staining of surface antigens fresh or thawed cells were incubated 30 minutes at +4c with antibodies and with Live/dead Fixable Green Dead Cell Stain (at dilution of 1:500; ThermoFisher) that were diluted in in Brilliant Stain Buffer (BD Bicoscience). When applicable the cells were incubated with MR-1 tetramer (1:2500) in +37c for 45 minutes and washed before continuing to other surface markers. After surface staining for detection of transcription factors and Ki67 the cells were permeabilized with FoxP3 transcription factor staining set (eBioscience) and of intracellular cytokines with Fixation/Permeabilisation Solution kit (BD Bioscience) as instructed by manufacturer. The samples were run using LSR Fortessa (BD Biosciences) and analyzed with FlowJo (BD Biosciences, LLC). The gating was

mostly done using biological negative populations but fluorescence minus one controls were also used when applicable. The antibodies used in the study are shown in Table S5. Optimal concentration for antibodies was titrated with live PBMCs.

Cell separation

Purification of $CD3^+$ T cells or $CD8^+$ T - cells from freshly isolated PBMCs was done with Pan T cell or CD8 Microbead isolation kit using LS Columns (both Miltenyi Biotec). Purity of $CD3^+$ cells was on average 97 (+/-1,2)% purity and CD8s 93 (+/-5,1)%. $CD4^+CD25^+CD127^-$ cells were sorted from freshly isolated PBMC with BD FACSAria II instrument (BD Biosciences). Prior sorting CD4 cells were enriched with Human $CD4^+$ T Cell Enrichment Cocktail (Stemcell Technologies) when isolating $CD4^+CD25^+CD127^-$ for suppression analysis.

IL-2 induced STAT5 phosphorylation

Thawed PBMCs were allowed to recover for 16 hours in complete medium and seeded at 150,000 cells per well in 96-well plates at a volume of 100 µL in complete medium. After 30 minutes of incubation at 37°C, cells were stimulated with IL-2 (200 U/mL for 7.5, 15 or 30 minutes and fixed for 10 minutes at 37°C with prewarmed 2% paraformaldehyde. Cells were washed twice and permeabilized with prechilled (-20°C) BD Phosflow Perm Buffer III (BD Biosciences) as instructed by the manufacturer.

Evaluation of Treg suppressor capacity

$CD4^+CD25^+CD127^-$ Treg cells were incubated for 6 days with carboxyfluorescein diacetate succinimidyl ester–labeled autologous responder T cells in ratio of 1:1. Anti-CD3/anti-CD28 beads (Life Technologies) were used as stimulus. $CD4^+$ cells were analyzed and the suppression percentage was calculated with the following formula: 100 – ([% proliferation in presence of Treg/% proliferation in absence of Treg] × 100).

620

621 **T cell activation cultures**

622 TCR activation for freshly isolated cells in vitro was done in flat-bottom plate coated with
623 unconjugated CD3- and CD28-antibodies (Immunotools) and cells were cultured in CTL test
624 media (Immunospot). After overnight stimulation Brefeldin A (BD Biosciences) was added for
625 the last 6 hours of stimulation after which the cells were collected for intracellular cytokine
626 staining. Similar stimulation without brefeldin was done for RNASeq. After 24h stimulation
627 cells were collected for RNAseq and stored at -80c before analysis.

628 MAIT cell stimulation with *E. coli* and *Candida albicans* was done as previously
629 described(*43*). Briefly, microbes were fixed with CellFIX (BD Biosciences) and added to the
630 cell culture in concentration of 6 x10^6 CFU for *E. coli* and 3 x10^6 CFU for *C. albicans*.
631 Unconjugated anti-CD28 antibody was added after one hour of culture with the fixed microbes.
632 Cells were incubated for a total of 24 hrs. For a positive control, a commercial PMA/ionomycin
633 preparation was used (Leukocyte Activation Cocktail, with BD GolgiPlug™ , BD Biosciences)
634 for six hours.

635

636 **siRNA Knockdown of Helios**

637 Freshly purified CD3+ T cells from 4 healthy donors were transfected following the
638 Amaxa™ 4D-Nucleofector™ Protocol for Unstimulated Human T Cells. T cells with 0.75 uM
639 of AllStars Negative Control siRNA (Qiagen) or the FlexiTube GeneSolution Helios-targeted
640 siRNA (Qiagen, Cat: SI00779044). Straight after, the cells were stimulated using Dynabeads™
641 Human Activator CD3/CD28 for T Cell Expansion and Activation (ThermoFisher) at a 1:2
642 ratio of beads to cell, for 24hs and Brefeldin A for last 6 hours for cytokine staining. Samples
643 with over -0.8 log2 fold change reduction in IKZF2 expression as measured by Nanostring
644 were qualified for further analysis (n=3) (Fig S7E).

645

NanoString analysis of patient PBMCs

RNA extraction was performed with RNeasy Mini Kit (Qiagen Hilden) as instructed by manufacturer from snap-frozen PBMCs, and 100 ng RNA in 5 μl volume was taken for NanoString gene expression analysis (NanoString Technologies). Our custom gene set consisted of 45 genes targeting IFN-regulated genes, JAK/STAT and NF-$\varkappa$B signaling related genes. Also five housekepping genes were included in the analysis. Further details of the code set, hybridization, scanning and data analysis are described elsewhere(*28*).

3' RNA-seq

RNA extraction was done with Qiagen miRNeasy Micro Kit (Qiagen Hilden). Quality and quantity of the extracted RNA samples was analyzed with 2100 Bioanalyzer using RNA 6000 Pico Kit (Agilent, Santa Clara, CA, USA). Single-indexed mRNA libraries were prepared with minimum input of each sample with QuantSeq 3' mRNA-Seq Library Prep Kit FWD (Lexogen Gmbh) according to user guide version 015UG009V0240 or 015UG009V0220. For CD3+ and Treg samples, globin mRNAs were removed from samples with Globin Block Module (Lexogen) and 6 bp Unique Molecular Identifiers (UMI) introduced with UMI Second Strand Synthesis Module (Lexogen) for detection and removal of PCR duplicates. Quality of libraries was measured using 2100 Bioanalyzer DNA High Sensitivity Kit (Agilent). Sequencing was performed with HiSeq 2500 System (Illumina) in high output run mode using v4 chemistry. Read length for the paired-end run was 2x101 bp and target coverage of 5 M reads for each library. QuantSeq 3' mRNA-Seq Integrated Data Analysis Pipeline on Bluebee® (Lexogen Gmbh) was used for preliminary quality evaluation of the RNA sequencing data and to obtain gene specific read counts. Data were analyzed utilizing Chipster v3.14 (*58*). Differential expression analysis was done using EdgeR for multivariate experiments either with 1 main effect (disease status in analysis of non-treated samples) or with two main effects (disease status and sample pairs in treated vs. untreated analysis) with TMM-normalization using Log2

transformation. Genes with <5 counts in <2 samples were removed from analyses. An adjusted p-value (FDR) of 0.05 was used as a limit for significantly differentially expressed genes. Correlation and volcano plots were generated using the ggplot2 package in R. Pathway analysis was done with Ingenuity Pathway Analysis (QIAGEN).

Inflammasome activation

Thawn human PBMCs were suspended in RPMI 1640 (Biowhittaker/Lonza) media, supplemented with 25 mM HEPES (Lonza), 100 U/ml penicillin and 100 μg/ml streptomycin, L-glutamine and 10% fetal calf serum (all from Gibco) and incubated o/n at +37°C. The cells were first stimulated with 1 μg/ml LPS (Sigma) for 4 hours and thereafter the NLRP3 inflammasome was activated by using 5 mM neutralized ATP (Sigma) for 45 min.

ELISA kit for IL-1β (high sensitivity, ThermoFisher) was used as instructed by the manufacturer to quantify cytokine concentrations from serum. Serum calprotectin levels were measured with clinically validated test in HUSLAB (Helsinki University Hospital, Helsinki, Finland). The mature, cleaved form of IL-1β was measured from cell culture supernatants using Human IL-1β/IL-1F2 DuoSet ELISA (R&D Systems). Cell death was analyzed from the cell culture supernatants using lactate dehydrogenase detection kit (Roche Diagnostics).

After inflammasome activation, total cellular RNA was purified using RNeasy Plus Mini kit (Qiagen), followed by cDNA synthesis with iScript kit (BioRad). Quantitative PCR was performed from 5 ng of cDNA per reaction using HOT FIREPol Evagreen qPCR SuperMix (Solis BioDyne) and LightCycler96 instrument (Roche). See Table S5 for the primer sequences. Relative gene expression was calculated using the 2(-ΔΔCt) method using *RPLP0* and *CASC3* as the housekeeping genes.

TSDR methylation analysis

Methylation status of the FoxP3 TSDR was done as previously described(*59*). For short, genomic DNA was isolated using the QIAsymphony system (Qiagen). Bisulfite conversion of nonmethylated cytosine residues to uracil was done using the EZ DNA Methylation Gold Kit (Zymo Research, Irvine, CA), according to the manufacturer's instructions. Demethylation status of the TSDR (Treg specific demethylated region) was determined by amplifying it with methylation-status sensitive primer/probe sets using the Bio-Rad iCycler real-time quantitative PCR instrument, as previously described (*60*). The data are shown on a relative scale as change of Ct: ΔCt = Ct (demethylated DNA) – Ct (methylated DNA).

Histology

The immunohistochemistry stainings of lymph node biopsies were performed in HUSLAB Pathology Department (Helsinki University Hospital, Helsinki, Finland) with clinically validated antibodies and protocols.

Auto-antibodies

Autoantibodies were measured as previously described with luciferase immunoprecipitation analysis(*36*)**.**

Legends

Fig 1. **Truncating variant of *IKZF2* disrupts the protein-protein interactions of Helios.** (A) Schematic representation of Helios protein. Blue arrow indicates the Y200X variant. (B) Immunoblot showing abundance of Helios in patients and healthy controls, respectively, in unstimulated PBMC and in PBMC after 3 and 7 days of anti-CD3-CD28 stimulation supplemented with IL-2. Band intensities were normalized to total protein stain intensity (Fig S1B) and relative values calculated by dividing with the average of the unstimulated controls. We validated that our antibody detects p.Y200X truncated protein (Fig S1C), but could not detect any from patient cells. (C) Helios expression in $CD4^+$ and $CD8^+$ T cells in patients compared to healthy controls. Histograms with patients and representative healthy control and (D) fluorescence intensity (MFI) of transcription factors Helios, Aiolos, and Ikaros for patients and healthy controls in $CD4^+$ and $CD8^+$ T cells are shown. (E) Abundance of protein partners of wild-type (wt) Helios' (orange) and variant Y200X (blue) Helios in interactome analysis. (F) A co-immunoprecipitation (Co-IP) assay displaying ability of HA tagged wild type Helios or variant Y200X Helios to form dimers with either Ikaros (IKZF1) or Aiolos (IKZF3) tagged with V5. (G) The proteins whose protein-protein interactions were altered in Y200X compared to wild type Helios were selected and ClueGo clustering was performed to show the biological processes they were involved at. Gating strategy for C&D are shown in Figure S1D. Cont./C= control, P1=patient 1, P2=patient 2

Fig 2. **Chronically activated T cells in patients with *IKZF2* p.Y200X variant.** (A) CD28 and CD27 expressing populations in patients and healthy controls (n=6) is shown in $CD4^+$ and $CD8^+$ T cells, respectively. (B) Relative abundance of naive $CD27^+CD28^+CD45RA^+CCR7^+$ cells and terminally differentiated $CD27^-CD28^-CD57^+CD45RA^-CCR7^-$ effector memory cells in patients and healthy controls and healthy relatives in $CD4^+$ and $CD8^+$ T cells, respectively. (C) Nanostring expression analysis of patients' PBMCs showing

differentially expressed genes compared to healthy controls. Log2 fold change to age and sex matched healthy control is shown. (D) Volcano plot of results from EdgeR analysis of $CD8^+$ T cell 3'RNA-seq data. Orange dots represents genes showing significant (FDR<0.05) differential expression between patients and age and sex matched controls (n=3). (E) Levels of IL-1β from culture supernatants containing unstimulated PBMC from patients and healthy controls, respectively. Gating strategy for A&B are shown in Figure S2A. Cont.= control, P1=patient 1, P2=patient 2

Fig 3. **TCR activation leads to increased proinflammatory response in T cells of patients with *IKZF2* p.Y200X variant.**

(A) Expression of Helios in $CD4^+$ and $CD8^+$ cells, respectively, after TCR stimulation with immobilized anti-CD3/CD28 antibodies in patients and healthy controls. Histograms of Helios expression in response to stimulation in $CD8^+$ T cells are shown in Figure S4B. (B) Correlation in $CD3^+$ T cell transcriptional regulation in response to 24 hour anti-CD3/CD28 stimulation between patients and healthy controls (n=5). Differential expression in unstimulated versus anti-CD3-CD28 stimulated cells and patients versus controls were analyzed from 3'RNA-seq data using EdgeR. Fitted linear regression is shown as a red dashed line (correlation coefficient 0.8). Genes found differentially upregulated or downregulated in patients versus controls in stimulated cells are marked in red and blue, respectively. (C) Percentage of both $CD4^+$ and $CD8^+$ T cells positive for IFNγ and IL-2, respectively, in patients compared to healthy controls after anti-CD3/CD28 stimulation and (D) dot plot of IFNγ and IL-2 expression in $CD4^+$ cells of healthy control and patient 2 are shown. (E) Expression of IL-2 receptor alpha chain CD25 in $CD4^+$ and $CD8^+$ T cells ex vivo. (F) Relative abundance of cells expressing CD69, CD25, PD1 or Ki-67 in $CD4^+$ T cells and (G) of cells expressing PD-1 or Ki-67 in $CD8^+$ T cells in patients and healthy controls after anti-CD3/CD28 stimulation. Gating strategy for A and E-G

765 are shown in Figure S4A and for C&D in Figure S5A&B. P1=patient 1, P2=patient 2, (blue
766 triangles), MFI=mean fluorescence intensity. Controls = open circles.
767
768 Fig 4. **Tregs of patients with *IKZF2* p.Y200X variant are activated and produce**
769 **proinflammatory cytokines.**
770 (A) Proportion of regulatory T cells (Treg) of $CD4^+$ cells gated as $CD127^-CD25^+FOXP3^+$ to
771 include also naive cells, $CD127^-CD25^{hi}FOXP3^{hi}$ or $CD127^-CD25^{hi}FOXP3^{hi}HELIOS^+$ in patients,
772 healthy relatives and healthy controls. (B) Relative abundance of recent thymic emigrant
773 $CD45RA^{hi}CD31^+$, naive $CD45RA^+$, and memory $CD45^-CCR7^+$ and $CD45RA^-CCR7^-$ cells in
774 $CD127^-CD25^+FOXP3^+$ Tregs in patients and healthy controls. (C) The suppression assay
775 showing suppressive capacity of Tregs of patients and of healthy controls. (D) Expression of
776 CTLA-4 and CD39 in $CD127^-CD25^+FOXP3^+$ Tregs in patients and healthy controls. (E) Portion
777 of $IL\text{-}2^+$ and $IFN\gamma^+$ cells, respectively, in both $Helios^-$ and $Helios^+$ Treg subsets in patients and
778 healthy controls after overnight stimulation with immobilized anti-CD3-CD28 antibodies. (F)
779 Volcano plot showing differentially expressed genes (orange dots) between patients and
780 healthy controls from EdgeR analysis of 3'RNA-seq data from purified $CD4^+CD25^{hi}CD127^-$
781 Tregs. (G) Portion of $IL\text{-}2^+$ and $IFN\gamma^+$ cells, respectively, in $CD4^+CD25^+FOXP3^+$ Tregs and (H)
782 $CD4^+FOXP3^-$ effector cells of healthy donors (n=3) modified with control silencing RNA
783 (siRNA) and Helios siRNA, respectively, and stimulated overnight with activating CD3-CD28
784 beads. (I) Mean fluorescence intensity (MFI) of CD25 in $CD4^+$ cells after same treatment.
785 Gating strategy for A is shown in Fig S6A, for B and D in Fig S6B, for E in Figure S5A&B
786 and for G-I in Fig S7A&B. P1=patient 1, P2=patient 2.
787
788 Fig 5. **Accumulation of Tfh cells in the perifollicular areas of lymph nodes.**
789 (A) Helios expression in lymph node $CD3^+CD4^+$ T cell was analyzed in $FOXP3^-$
790 $CXCR5^{low}PD1^{low}BCL\text{-}6^-$ T non-follicular helper (Tnonf), $CD4^+FOXP3^-CXCR5^{hi}PD1^{hi}BCL\text{-}6^+$ T

follicular helper (Tfh), $CD4^+FOXP3^+CXCR5^{low}PD1^{low}BCL\text{-}6^-$ T non-follicular regulatory (Treg) and $CD4^+FOXP3^+CXCR5^{hi}PD1^{hi}BCL\text{-}6^+$ T follicular regulator (Tfr) cells. Gating strategy in 19 year old male and (B) mean fluorescence intensity (MFI) of Helios for four individual donors is shown. (C) Frequency of $CD4^+$ T cells expressing follicular homing receptor $CXCR5^+$ in PBMCs of patients and healthy controls. (D) Histological analysis of patients' lymph nodes showed accumulation of CD3+ T cells (brown) in the perifollicular region around the B cell follicles containing CD20+ B cells (red). A more detailed immunohistochemistry staining of accumulated cells expressed with Tfh markers Bcl6 and PD-1 and Ki-67 indicating proliferation activity. (E) Auto-antibodies against cytokines in patient 2. Fold change compared to the mean of healthy controls (n=5) is shown. Gating strategy for A is shown in Fig S8A and for C in Fig S8B. Cont.= control, P1=patient 1, P2=patient 2

Fig 6**. Reduction of circulating MAIT cells.**

(A) Dot plots showing abundance of $V\alpha7.2^+CD161^+$ MAITs in the live $CD3^+$ T cells from peripheral blood in patients and representative healthy control and (B) their frequency in $CD3^+$ T cells in patients, healthy relatives and healthy controls. (C) Mean fluorescence intensity (MFI) of Helios in MAITs. (D) Abundance of $MR1^+$, $CD4^-CD8^+$ and $CD69^+$ cells, respectively, in MAITs in patients and healthy controls. (E) Frequency MAITs in colon and (F) in duodenum samples obtained from patients and organ donors without any chronic inflammatory conditions. (G) Helios expression in MAITs from PBMC in response to stimulation with *E. coli*, *Candida albicans* or PMA. Gating strategy for D is shown in Fig S10A and for E&F in S10D. P1=patient 1, P2=patient 2.

Table 1. **Clinical presentation and immunological phenotype of patients with the *IKZF2* p.Y200X variant**

Supplementary Materials:

Supplementary Clinical Data

Figure S1: Targeted capillary sequencing of *IKZF2* and gating strategy to measure Ikaros family transcription factors

Figure S2: Gating strategy to measure different T and B cell maturation phases and Helios expression in them

Figure S3: Inflammasome activation in patients with the *IKZF2* p.Y200X variant

Figure S4: Gating strategy and volcano plots of T cell activation experiments

Figure S5: Gating strategy to cytokine staining

Figure S6: Gating strategy to regulatory T cell experiments

Figure S7: Gating strategy to siRNA experiment

Figure S8: Gating strategy to follicular T helper cell quantification and auto-antibodies in patient 1

Figure S9: NK cell phenotype in patients with the *IKZF2* p.Y200X variant

Figure S10: Gating strategy to MAIT experiments

Table S1: Whole exome sequencing and filtration of data

Table S2: Protein-protein interactions of Helios identified in biotin proximity ligation and ClueGo clustering of the results

Table S3: List of differentially expressed genes in different RNAseq conditions

Table S4: Pathway analysis of RNAseq data trough IPA

Table S5: Supplementary list of reagents

Table S6: Raw data from figures

References and notes

1. A. Rebollo, C. Schmitt, Ikaros, Aiolos and Helios: transcription regulators and lymphoid malignancies. *Immunol. Cell Biol.* **81**, 171–175 (2003).

2. J. Kim, S. Sif, B. Jones, A. Jackson, J. Koipally, E. Heller, S. Winandy, A. Viel, A. Sawyer, T. Ikeda, R. Kingston, K. Georgopoulos, Ikaros DNA-binding proteins direct formation of chromatin remodeling complexes in lymphocytes. *Immunity.* **10**, 345–355 (1999).

3. R. Sridharan, S. T. Smale, Predominant interaction of both Ikaros and Helios with the NuRD complex in immature thymocytes. *J. Biol. Chem.* **282**, 30227–30238 (2007).

4. K. Georgopoulos, The making of a lymphocyte: the choice among disparate cell fates and the IKAROS enigma. *Genes Dev.* **31**, 439–450 (2017).

5. S. Asanuma, M. Yamagishi, K. Kawanami, K. Nakano, A. Sato-Otsubo, S. Muto, M. Sanada, T. Yamochi, S. Kobayashi, A. Utsunomiya, M. Iwanaga, K. Yamaguchi, K. Uchimaru, S. Ogawa, T. Watanabe, Adult T-cell leukemia cells are characterized by abnormalities of Helios expression that promote T cell growth. *Cancer Sci.* **104**, 1097–1106 (2013).

6. S.-M. Park, H. Cho, A. M. Thornton, T. S. Barlowe, T. Chou, S. Chhangawala, L. Fairchild, J. Taggart, A. Chow, A. Schurer, A. Gruet, M. D. Witkin, J. H. Kim, E. M. Shevach, A. Krivtsov, S. A. Armstrong, C. Leslie, M. G. Kharas, IKZF2 Drives Leukemia Stem Cell Self-Renewal and Inhibits Myeloid Differentiation. *Cell Stem Cell.* **24**, 153–165.e7 (2019).

7. H. S. Kuehn, B. Boisson, C. Cunningham-Rundles, J. Reichenbach, A. Stray-Pedersen, E. W. Gelfand, P. Maffucci, K. R. Pierce, J. K. Abbott, K. V. Voelkerding, S. T. South, N. H. Augustine, J. S. Bush, W. K. Dolen, B. B. Wray, Y. Itan, A. Cobat, H. S. Sorte, S. Ganesan, S. Prader, T. B. Martins, M. G. Lawrence, J. S. Orange, K. R. Calvo, J. E. Niemela, J.-L. Casanova, T. A. Fleisher, H. R. Hill, A. Kumánovics, M. E. Conley, S. D. Rosenzweig, Loss of B Cells in Patients with Heterozygous Mutations in IKAROS. *N. Engl. J. Med.* **374**, 1032–1043 (2016).

8. D. Boutboul, H. S. Kuehn, Z. Van de Wyngaert, J. E. Niemela, I. Callebaut, J. Stoddard, C. Lenoir, V. Barlogis, C. Farnarier, F. Vely, N. Yoshida, S. Kojima, H. Kanegane, A. Hoshino, F. Hauck, L. Lhermitte, V. Asnafi, P. Roehrs, S. Chen, J. W. Verbsky, K. R. Calvo, A. Husami, K. Zhang, J. Roberts, D. Amrol, J. Sleaseman, A. P. Hsu, S. M. Holland, R. Marsh, A. Fischer, T. A. Fleisher, C. Picard, S. Latour, S. D. Rosenzweig, Dominant-negative IKZF1 mutations cause a T, B, and myeloid cell combined immunodeficiency. *J. Clin. Invest.* **128**, 3071–3087 (2018).

9. H. S. Kuehn, J. E. Niemela, J. Stoddard, S. C. Mannurita, T. Shahin, S. Goel, M. Hintermeyer, R. J. Heredia, M. Garofalo, L. Lucas, S. Singh, A. Tondo, Z. Jacobs, W. A. Gahl, S. Latour, J. Verbsky, J. Routes, C. Cunningham-Rundles, K. Boztug, E. Gambineri, T. A. Fleisher, S. Chandrakasan, S. D. Rosenzweig, Germline IKAROS dimerization haploinsufficiency causes hematologic cytopenias and malignancies. *Blood.* **137**, 349–363 (2021).

10. Q. Cai, A. Dierich, M. Oulad-Abdelghani, S. Chan, P. Kastner, Helios deficiency has minimal impact on T cell development and function. *J. Immunol.* **183**, 2303–2311 (2009).

881 21. H.-J. Kim, R. A. Barnitz, T. Kreslavsky, F. D. Brown, H. Moffett, M. E. Lemieux, Y.
882 Kaygusuz, T. Meissner, T. A. W. Holderried, S. Chan, P. Kastner, W. N. Haining, H. Cantor,
883 Stable inhibitory activity of regulatory T cells requires the transcription factor Helios.
884 *Science*. **350**, 334–339 (2015).

885 22. M. Sebastian, M. Lopez-Ocasio, A. Metidji, S. A. Rieder, E. M. Shevach, A. M. Thornton,
886 Helios Controls a Limited Subset of Regulatory T Cell Functions. *J. Immunol.* **196**, 144–155
887 (2016).

888 23. M. S. F. Ng, T. L. Roth, V. F. Mendoza, A. Marson, T. D. Burt, Helios enhances the
889 preferential differentiation of human fetal CD4+ naïve T cells into regulatory T cells. *Sci*
890 *Immunol*. **4** (2019), doi:10.1126/sciimmunol.aav5947.

891 24. I. Baine, S. Basu, R. Ames, R. S. Sellers, F. Macian, Helios induces epigenetic silencing of
892 IL2 gene expression in regulatory T cells. *J. Immunol.* **190**, 1008–1016 (2013).

893 25. H. Nakagawa, J. M. Sido, E. E. Reyes, V. Kiers, H. Cantor, H.-J. Kim, Instability of Helios-
894 deficient Tregs is associated with conversion to a T-effector phenotype and enhanced
895 antitumor immunity. *Proc. Natl. Acad. Sci. U. S. A.* **113**, 6248–6253 (2016).

896 26. M. E. Himmel, K. G. MacDonald, R. V. Garcia, T. S. Steiner, M. K. Levings, Helios+ and
897 Helios- cells coexist within the natural FOXP3+ T regulatory cell subset in humans. *J.*
898 *Immunol.* **190**, 2001–2008 (2013).

899 27. T. Akimova, U. H. Beier, L. Wang, M. H. Levine, W. W. Hancock, Helios expression is a
900 marker of T cell activation and proliferation. *PLoS One*. **6**, e24226 (2011).

901 28. C. Peters, H.-H. Oberg, D. Kabelitz, D. Wesch, Phenotype and regulation of
902 immunosuppressive Vδ2-expressing γδ T cells. *Cell. Mol. Life Sci.* **71**, 1943–1960 (2014).

903 29. K. Serre, C. Bénézech, G. Desanti, S. Bobat, K.-M. Toellner, R. Bird, S. Chan, P. Kastner, A.
904 F. Cunningham, I. C. M. Maclennan, E. Mohr, Helios is associated with CD4 T cells
905 differentiating to T helper 2 and follicular helper T cells in vivo independently of Foxp3
906 expression. *PLoS One*. **6**, e20731 (2011).

907 30. T. A. Doering, A. Crawford, J. M. Angelosanto, M. A. Paley, C. G. Ziegler, E. J. Wherry,
908 Network analysis reveals centrally connected genes and pathways involved in CD8+ T cell
909 exhaustion versus memory. *Immunity*. **37**, 1130–1144 (2012).

910 31. A. Crawford, J. M. Angelosanto, C. Kao, T. A. Doering, P. M. Odorizzi, B. E. Barnett, E. J.
911 Wherry, Molecular and transcriptional basis of CD4+ T cell dysfunction during chronic
912 infection. *Immunity*. **40**, 289–302 (2014).

913 32. E. V. Davydov, D. L. Goode, M. Sirota, G. M. Cooper, A. Sidow, S. Batzoglou, Identifying a
914 high fraction of the human genome to be under selective constraint using GERP++. *PLoS*
915 *Comput. Biol.* **6**, e1001025 (2010).

916 33. K. J. Roux, D. I. Kim, B. Burke, *Curr. Protoc. Protein Sci.*, in press.

917 34. X. Liu, K. Salokas, F. Tamene, Y. Jiu, R. G. Weldatsadik, T. Öhman, M. Varjosalo, An AP-
918 MS- and BioID-compatible MAC-tag enables comprehensive mapping of protein interactions
919 and subcellular localizations. *Nat. Commun.* **9**, 1188 (2018).

921 25. T. Yoshida, K. Georgopoulos, Ikaros fingers on lymphocyte differentiation. *Int. J. Hematol.*
922 **100**, 220–229 (2014).

923 26. C. Dege, J. Hagman, Mi-2/NuRD chromatin remodeling complexes regulate B and T-
924 lymphocyte development and function. *Immunol. Rev.* **261**, 126–140 (2014).

925 27. G. Bindea, B. Mlecnik, H. Hackl, P. Charoentong, M. Tosolini, A. Kirilovsky, W.-H.
926 Fridman, F. Pagès, Z. Trajanoski, J. Galon, ClueGO: a Cytoscape plug-in to decipher
927 functionally grouped gene ontology and pathway annotation networks. *Bioinformatics.* **25**,
928 1091–1093 (2009).

929 28. S. Keskitalo, E. Haapaniemi, E. Einarsdottir, K. Rajamäki, H. Heikkilä, M. Ilander, M.
930 Pöyhönen, E. Morgunova, K. Hokynar, S. Lagström, S. Kivirikko, S. Mustjoki, K. Eklund, J.
931 Saarela, J. Kere, M. R. J. Seppänen, A. Ranki, K. Hannula-Jouppi, M. Varjosalo, Novel
932 TMEM173 Mutation and the Role of Disease Modifying Alleles. *Front. Immunol.* **10**, 2770
933 (2019).

934 29. M. Pruenster, T. Vogl, J. Roth, M. Sperandio, S100A8/A9: From basic science to clinical
935 application. *Pharmacol. Ther.* **167**, 120–131 (2016).

936 30. A. Åsberg, L. Løfblad, A. Felic, G. G. Hov, Measuring calprotectin in plasma and blood with
937 a fully automated turbidimetric assay. *Scand. J. Clin. Lab. Invest.*, 1–8 (2019).

938 31. M. Frosch, M. Ahlmann, T. Vogl, H. Wittkowski, N. Wulffraat, D. Foell, J. Roth, The
939 myeloid-related proteins 8 and 14 complex, a novel ligand of toll-like receptor 4, and
940 interleukin-1beta form a positive feedback mechanism in systemic-onset juvenile idiopathic
941 arthritis. *Arthritis Rheum.* **60**, 883–891 (2009).

942 32. F. Sallusto, J. Geginat, A. Lanzavecchia, Central memory and effector memory T cell
943 subsets: function, generation, and maintenance. *Annu. Rev. Immunol.* **22**, 745–763 (2004).

944 33. M. Pesu, W. T. Watford, L. Wei, L. Xu, I. Fuss, W. Strober, J. Andersson, E. M. Shevach, M.
945 Quezado, N. Bouladoux, A. Roebroek, Y. Belkaid, J. Creemers, J. J. O'Shea, T-cell-
946 expressed proprotein convertase furin is essential for maintenance of peripheral immune
947 tolerance. *Nature.* **455**, 246–250 (2008).

948 34. R. Elhage, M. Cheraï, B. Levacher, G. Darrasse-Jeze, C. Baillou, X. Zhao, A.-M. Khatib, E.
949 Piaggio, D. Klatzmann, C-terminal cleavage of human Foxp3 at a proprotein convertase
950 motif abrogates its suppressive function. *Scand. J. Immunol.* **81**, 229–239 (2015).

951 35. T. Vincent, M. Plawecki, R. Goulabchand, P. Guilpain, J. F. Eliaou, Emerging clinical
952 phenotypes associated with anti-cytokine autoantibodies. *Autoimmun. Rev.* **14**, 528–535
953 (2015).

954 36. J. Kärner, A. Meager, M. Laan, J. Maslovskaja, M. Pihlap, A. Remm, E. Juronen, A. S. B.
955 Wolff, E. S. Husebye, K. T. Podkrajšek, N. Bratanic, T. Battelino, N. Willcox, P. Peterson,
956 K. Kisand, Anti-cytokine autoantibodies suggest pathogenetic links with autoimmune
957 regulator deficiency in humans and mice. *Clin. Exp. Immunol.* **171**, 263–272 (2013).

958 37. L. Mazzurana, M. Forkel, A. Rao, A. Van Acker, E. Kokkinou, T. Ichiya, S. Almer, C. Höög,
959 D. Friberg, J. Mjösberg, Suppression of Aiolos and Ikaros expression by lenalidomide

reduces human ILC3-ILC1/NK cell transdifferentiation. *Eur. J. Immunol.* **49**, 1344–1355 (2019).

38. A. Gibbs, E. Leeansyah, A. Introini, D. Paquin-Proulx, K. Hasselrot, E. Andersson, K. Broliden, J. K. Sandberg, A. Tjernlund, MAIT cells reside in the female genital mucosa and are biased towards IL-17 and IL-22 production in response to bacterial stimulation. *Mucosal Immunol.* **10**, 35–45 (2017).

39. A. J. Corbett, S. B. G. Eckle, R. W. Birkinshaw, L. Liu, O. Patel, J. Mahony, Z. Chen, R. Reantragoon, B. Meehan, H. Cao, N. A. Williamson, R. A. Strugnell, D. Van Sinderen, J. Y. W. Mak, D. P. Fairlie, L. Kjer-Nielsen, J. Rossjohn, J. McCluskey, T-cell activation by transitory neo-antigens derived from distinct microbial pathways. *Nature.* **509**, 361–365 (2014).

40. J. Dias, C. Boulouis, J.-B. Gorin, R. H. G. A. van den Biggelaar, K. G. Lal, A. Gibbs, L. Loh, M. Y. Gulam, W. R. Sia, S. Bari, W. Y. K. Hwang, D. F. Nixon, S. Nguyen, M. R. Betts, M. Buggert, M. A. Eller, K. Broliden, A. Tjernlund, J. K. Sandberg, E. Leeansyah, The CD4-CD8- MAIT cell subpopulation is a functionally distinct subset developmentally related to the main CD8+ MAIT cell pool. *Proc. Natl. Acad. Sci. U. S. A.* **115**, E11513–E11522 (2018).

41. N.-E. Serriari, M. Eoche, L. Lamotte, J. Lion, M. Fumery, P. Marcelo, D. Chatelain, A. Barre, E. Nguyen-Khac, O. Lantz, J.-L. Dupas, E. Treiner, Innate mucosal-associated invariant T (MAIT) cells are activated in inflammatory bowel diseases. *Clin. Exp. Immunol.* **176**, 266–274 (2014).

42. D. I. Godfrey, H.-F. Koay, J. McCluskey, N. A. Gherardin, The biology and functional importance of MAIT cells. *Nat. Immunol.* **20**, 1110–1128 (2019).

43. J. Dias, J. K. Sandberg, E. Leeansyah, Extensive Phenotypic Analysis, Transcription Factor Profiling, and Effector Cytokine Production of Human MAIT Cells by Flow Cytometry. *Methods Mol. Biol.* **1514**, 241–256 (2017).

44. D. Holzinger, K. Tenbrock, J. Roth, Alarmins of the S100-Family in Juvenile Autoimmune and Auto-Inflammatory Diseases. *Front. Immunol.* **10**, 182 (2019).

45. A. M. Thornton, J. Lu, P. E. Korty, Y. C. Kim, C. Martens, P. D. Sun, E. M. Shevach, Helios+ and Helios- Treg subpopulations are phenotypically and functionally distinct and express dissimilar TCR repertoires. *Eur. J. Immunol.* (2019), doi:10.1002/eji.201847935.

46. H. Bendfeldt, M. Benary, T. Scheel, K. Steinbrink, A. Radbruch, H. Herzel, R. Baumgrass, IL-2 Expression in Activated Human Memory FOXP3(+) Cells Critically Depends on the Cellular Levels of FOXP3 as Well as of Four Transcription Factors of T Cell Activation. *Front. Immunol.* **3**, 264 (2012).

47. L. A. Vella, M. Buggert, S. Manne, R. S. Herati, I. Sayin, L. Kuri-Cervantes, I. Bukh Brody, K. C. O'Boyle, H. Kaprielian, J. R. Giles, S. Nguyen, A. Muselman, J. P. Antel, A. Bar-Or, M. E. Johnson, D. H. Canaday, A. Naji, V. V. Ganusov, T. M. Laufer, A. D. Wells, Y. Dori, M. G. Itkin, M. R. Betts, E. J. Wherry, T follicular helper cells in human efferent lymph retain lymphoid characteristics. *J. Clin. Invest.* **129**, 3185–3200 (2019).

998. E. W. Meermeier, M. J. Harriff, E. Karamooz, D. M. Lewinsohn, MAIT cells and microbial immunity. *Immunol. Cell Biol.* **96**, 607–617 (2018).

999. A. Willing, O. A. Leach, F. Ufer, K. E. Attfield, K. Steinbach, N. Kursawe, M. Piedavent, M. A. Friese, CD8- MAIT cells infiltrate into the CNS and alterations in their blood frequencies correlate with IL-18 serum levels in multiple sclerosis. *Eur. J. Immunol.* **44**, 3119–3128 (2014).

1000. A. Chiba, N. Tamura, K. Yoshikiyo, G. Murayama, M. Kitagaichi, K. Yamaji, Y. Takasaki, S. Miyake, Activation status of mucosal-associated invariant T cells reflects disease activity and pathology of systemic lupus erythematosus. *Arthritis Res. Ther.* **19**, 58 (2017).

1001. T. J. Break, V. Oikonomou, N. Dutzan, J. V. Desai, M. Swidergall, T. Freiwald, D. Chauss, O. J. Harrison, J. Alejo, D. W. Williams, S. Pittaluga, C.-C. R. Lee, N. Bouladoux, M. Swamydas, K. W. Hoffman, T. Greenwell-Wild, V. M. Bruno, L. B. Rosen, W. Lwin, A. Renteria, S. M. Pontejo, J. P. Shannon, I. A. Myles, P. Olbrich, E. M. N. Ferré, M. Schmitt, D. Martin, Genomics and Computational Biology Core, D. L. Barber, N. V. Solis, L. D. Notarangelo, D. V. Serreze, M. Matsumoto, H. D. Hickman, P. M. Murphy, M. S. Anderson, J. K. Lim, S. M. Holland, S. G. Filler, B. Afzali, Y. Belkaid, N. M. Moutsopoulos, M. S. Lionakis, Aberrant type 1 immunity drives susceptibility to mucosal fungal infections. *Science*. **371** (2021), doi:10.1126/science.aay5731.

1002. K. Wang, M. Li, H. Hakonarson, ANNOVAR: functional annotation of genetic variants from high-throughput sequencing data. *Nucleic Acids Res.* **38**, e164 (2010).

1003. K. J. Karczewski, L. C. Francioli, G. Tiao, B. B. Cummings, J. Alföldi, Q. Wang, R. L. Collins, K. M. Laricchia, A. Ganna, D. P. Birnbaum, L. D. Gauthier, H. Brand, M. Solomonson, N. A. Watts, D. Rhodes, M. Singer-Berk, E. M. England, E. G. Seaby, J. A. Kosmicki, R. K. Walters, K. Tashman, Y. Farjoun, E. Banks, T. Poterba, A. Wang, C. Seed, N. Whiffin, J. X. Chong, K. E. Samocha, E. Pierce-Hoffman, Z. Zappala, A. H. O'Donnell-Luria, E. V. Minikel, B. Weisburd, M. Lek, J. S. Ware, C. Vittal, I. M. Armean, L. Bergelson, K. Cibulskis, K. M. Connolly, M. Covarrubias, S. Donnelly, S. Ferriera, S. Gabriel, J. Gentry, N. Gupta, T. Jeandet, D. Kaplan, C. Llanwarne, R. Munshi, S. Novod, N. Petrillo, D. Roazen, V. Ruano-Rubio, A. Saltzman, M. Schleicher, J. Soto, K. Tibbetts, C. Tolonen, G. Wade, M. E. Talkowski, Genome Aggregation Database Consortium, B. M. Neale, M. J. Daly, D. G. MacArthur, The mutational constraint spectrum quantified from variation in 141,456 humans. *Nature*. **581**, 434–443 (2020).

1004. 1000 Genomes Project Consortium, A. Auton, L. D. Brooks, R. M. Durbin, E. P. Garrison, H. M. Kang, J. O. Korbel, J. L. Marchini, S. McCarthy, G. A. McVean, G. R. Abecasis, A global reference for human genetic variation. *Nature*. **526**, 68–74 (2015).

1005. J. T. Robinson, H. Thorvaldsdóttir, A. M. Wenger, A. Zehir, J. P. Mesirov, Variant Review with the Integrative Genomics Viewer. *Cancer Res.* **77**, e31–e34 (2017).

1006. D. Mellacheruvu, Z. Wright, A. L. Couzens, J.-P. Lambert, N. A. St-Denis, T. Li, Y. V. Miteva, S. Hauri, M. E. Sardiu, T. Y. Low, V. A. Halim, R. D. Bagshaw, N. C. Hubner, A. al-Hakim, A. Bouchard, D. Faubert, D. Fermin, W. H. Dunham, M. Goudreault, Z.-Y. Lin, B. G. Badillo, T. Pawson, D. Durocher, B. Coulombe, R. Aebersold, G. Superti-Furga, J. Colinge, A. J. R. Heck, H. Choi, M. Gstaiger, S. Mohammed, I. M. Cristea, K. L. Bennett, M. P. Washburn, B. Raught, R. M. Ewing, A.-C. Gingras, A. I. Nesvizhskii, The CRAPome: a

contaminant repository for affinity purification–mass spectrometry data. *Nat. Methods*. **10**, 730–736 (2013).

57. P. Shannon, A. Markiel, O. Ozier, N. S. Baliga, J. T. Wang, D. Ramage, N. Amin, B. Schwikowski, T. Ideker, Cytoscape: a software environment for integrated models of biomolecular interaction networks. *Genome Res*. **13**, 2498–2504 (2003).

58. M. A. Kallio, J. T. Tuimala, T. Hupponen, P. Klemelä, M. Gentile, I. Scheinin, M. Koski, J. Käki, E. I. Korpelainen, Chipster: user-friendly analysis software for microarray and other high-throughput data. *BMC Genomics*. **12**, 507 (2011).

59. R. Vanhanen, K. Leskinen, I. P. Mattila, P. Saavalainen, T. P. Arstila, Epigenetic and transcriptional analysis supports human regulatory T cell commitment at the CD4+CD8+ thymocyte stage. *Cell. Immunol*. **347**, 104026 (2020).

60. G. Wieczorek, A. Asemissen, F. Model, I. Turbachova, S. Floess, V. Liebenberg, U. Baron, D. Stauch, K. Kotsch, J. Pratschke, A. Hamann, C. Loddenkemper, H. Stein, H. D. Volk, U. Hoffmüller, A. Grützkau, A. Mustea, J. Huehn, C. Scheibenbogen, S. Olek, Quantitative DNA methylation analysis of FOXP3 as a new method for counting regulatory T cells in peripheral blood and solid tissue. *Cancer Res*. **69**, 599–608 (2009).

Acknowledgements

The MR1 tetramer technology was developed jointly by Dr. James McCluskey, Dr. Jamie Rossjohn, and Dr. David Fairlie, and the material was produced by the NIH Tetramer Core Facility as permitted to be distributed by the University of Melbourne. Sequencing library preparations, exome enrichment, and high-throughput sequencing of DNA and RNA samples was conducted at the Sequencing unit of the Institute for Molecular Medicine Finland Technology Centre. This study was supported by grants from Emil Aaltonen Foundation, Sigrid Juselius Foundation, Finnish Medical Foundation and Academy of Finland (grant 308913). The authors thank Tamas Bazsinka and Sini Miettinen for technical assistance.

IH designed and performed experiments, analyzed data, and wrote the original draft of the manuscript with EK.

MeK and MaK designed and performed experiments, analyzed data, and contributed to writing and editing of the manuscript.

NH, SK, SM, JoS, VG, NA, KaKe, RV, KN, JD, HS and KaKi designed and performed experiments, analyzed data, and contributed to editing of the manuscript

UO and JaSy acquired the samples and clinical data and contributed to editing of the manuscript

KE, MM, TPA, JB, PP, JaSa, MV designed experiments, analyzed data, and contributed to editing of the manuscript

EK coordinated the study, designed experiments, analyzed data, and wrote the original draft of the manuscript.

Competing interests

The authors declare that they have no competing interests.

Data availability

For access to the individual level genomics data please contact the data access committee (fimm-dac@helsinki.fi).

1089 **Table 1**

		Patient 1	Patient 2	Reference values (unit)
Sex		F	M	
Age		44	66	
Clinical features				
Aphtous ulcers (vaginal/oral)		x	x	
Thrush (oral/vaginal)		x	x	
Recurrent respiratory infections		x	x	
Hypothyreosis		x	x	
Vitiligo		x		
Lichen			x	
Lymphadenopathy		x	x	
Lymphoma			x	
Lymphocytes (% of leukocytes)		23	18	**(% of parent)**
T cells		74	51	66-88
CD4+		55	48	
CCR7+CD45RA+	naive	23	3	21-55
CCR7+CD45RA-	central memory	50	35	8-33
CCR7-CD45RA-	effector memory	24	55	20-52
CCR7-CD45RA+	effector memory RA+	3	8	1-17
CD38+HLADR+	activated	7	9	1-5
CD31+CD45RA+	recent thymic emigrant	11	0,4	14-38
CD8+		42	50	
CCR7+CD45RA+	naive	16	2	19-71
CCR7+CD45RA-	central memory	11	4	1-7
CCR7-CD45RA-	effector memory	29	54	15-63
CCR7-CD45RA+	effector memory RA+	44	40	4-34
CD38+HLADR+	activated	29	22	1-22
CD31+CD45RA+	recent thymic emigrant	12	0,5	17-65
TCRgd		1,4	0,7	2-12
TCRab+CD4-cd8-		1,4	0,2	3-9
NK cells		10	33	4-25
B cells		16	15	6-19
CD27-IgD+	naive	78	85	43-82
CD27+IgD+	unswitched memory	16,9	4,5	7,2-31
CD27+IgD-	class-switched memory	1,9	8,4	6,5-29
CD38lowCD21low	CD21low	18,8	2,9	1,1-6,9
CD38++IgM++	transtitional	7,7	11	0,6-3,5
CD38++IgM-	plasmablast/-cell	0	1,2	0,4-3,6
Antibody levels				**(g/l)**
IgG		4,32	10,16	6,77-15,0

IgG1	3,6	7,48	5,2-12,7
IgG2	0,64	1,84	1,43-5,6
IgG3	0,17	0,19	0,11-0,85
IgG4	<0,02	0,0003	0,03-2
IgM	0,22	1,82	0,88-4,84
IgA	0,59	0,69	0,36-2,59
IgE	3	<1	<1
Vaccine responses	low	normal	

1090
1091

Fig 1

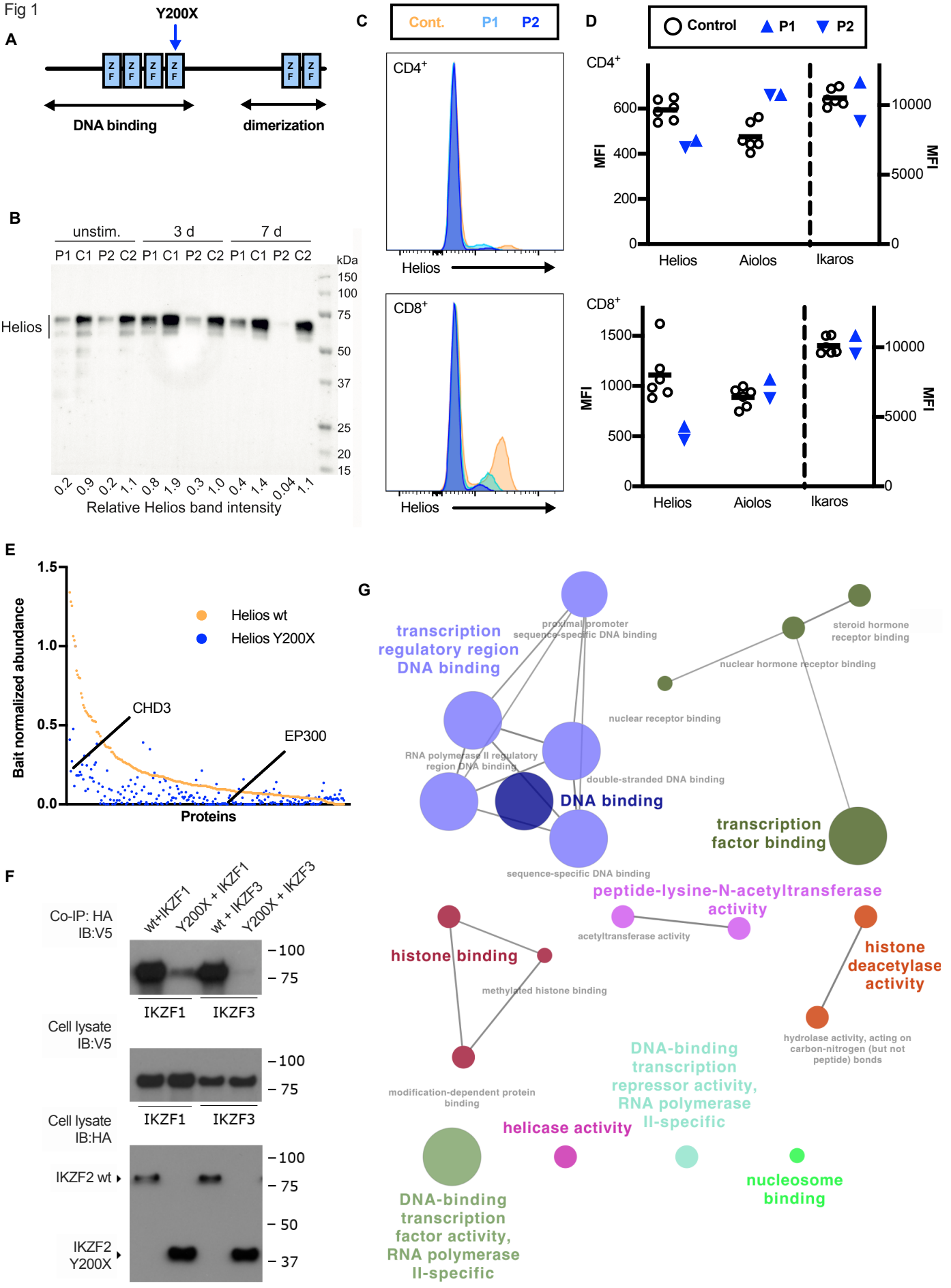
A
Y200X
ZF
DNA binding
dimerization
B
unstim.
3 d
7 d
P1 C1 P2 C2 P1 C1 P2 C2 P1 C1 P2 C2
kDa
150
100
75
50
37
25
20
15
Helios
0.2 0.9 0.2 1.1 0.8 1.9 0.3 1.0 0.4 1.4 0.04 1.1
Relative Helios band intensity
C
Cont.
P1
P2
CD4+
Helios
CD8+
Helios
D
Control
P1
P2
CD4+
MFI
600
400
200
0
10000
5000
0
Helios
Aiolos
Ikaros
CD8+
MFI
1500
1000
500
0
10000
5000
0
Helios
Aiolos
Ikaros
E
Bait normalized abundance
1.5
1.0
0.5
0.0
Helios wt
Helios Y200X
CHD3
EP300
Proteins
F
Co-IP: HA
IB:V5
wt+IKZF1
Y200X + IKZF1
wt + IKZF3
Y200X + IKZF3
100
75
IKZF1
IKZF3
Cell lysate
IB:V5
100
75
IKZF1
IKZF3
Cell lysate
IB:HA
IKZF2 wt
IKZF2
Y200X
100
75
50
37
G
transcription regulatory region DNA binding
proximal promoter sequence-specific DNA binding
steroid hormone receptor binding
nuclear hormone receptor binding
nuclear receptor binding
RNA polymerase II regulatory region DNA binding
double-stranded DNA binding
DNA binding
sequence-specific DNA binding
transcription factor binding
peptide-lysine-N-acetyltransferase activity
acetyltransferase activity
histone binding
methylated histone binding
histone deacetylase activity
hydrolase activity, acting on carbon-nitrogen (but not peptide) bonds
modification-dependent protein binding
DNA-binding transcription repressor activity, RNA polymerase II-specific
helicase activity
nucleosome binding
DNA-binding transcription factor activity, RNA polymerase II-specific

Fig 2

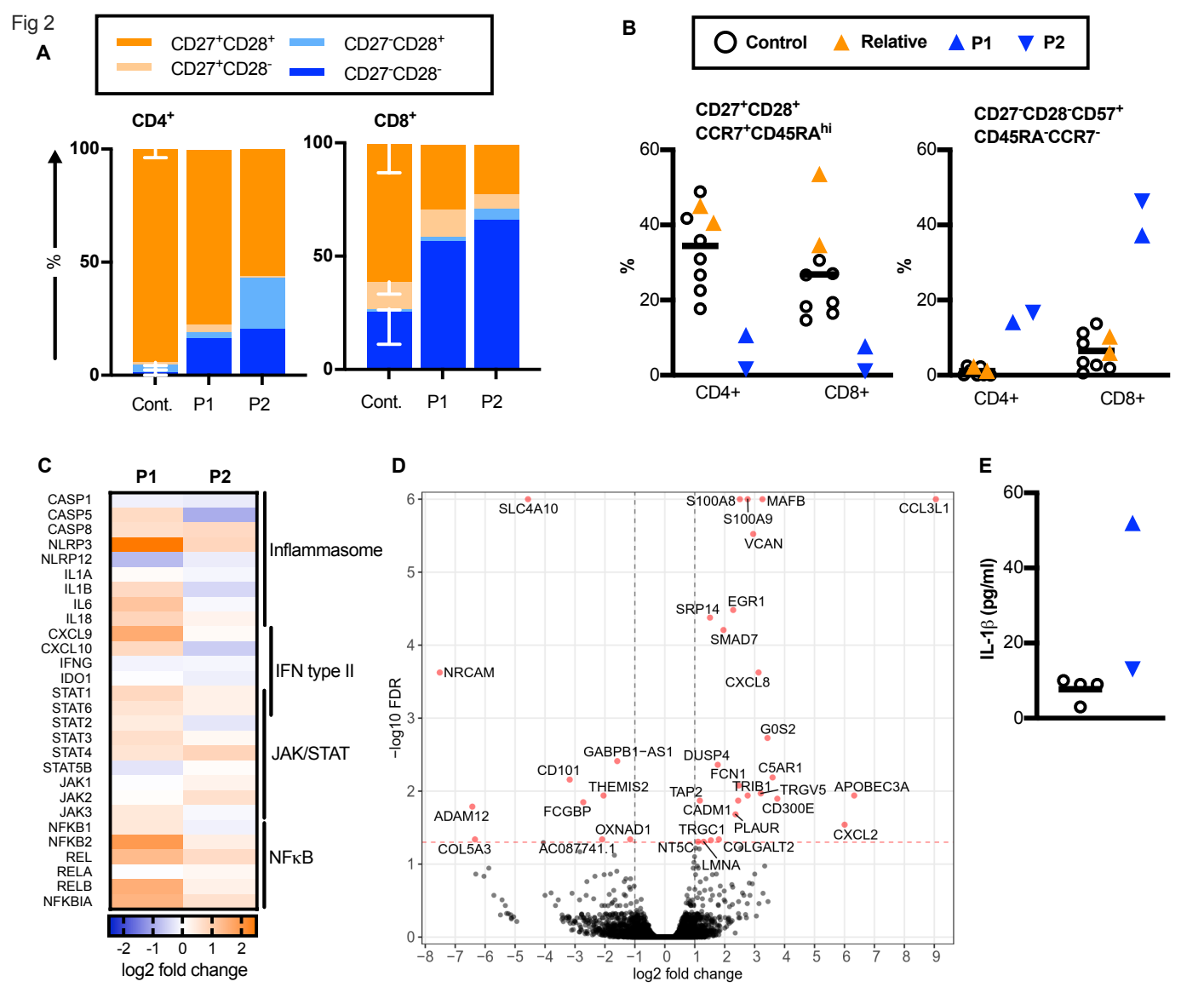
A
CD27+CD28+
CD27+CD28-
CD27-CD28+
CD27-CD28-
CD4+
CD8+
%
100
50
0
Cont.
P1
P2
B
Control
Relative
P1
P2
CD27+CD28+
CCR7+CD45RAhi
CD27-CD28-CD57+
CD45RA-CCR7-
60
40
20
0
CD4+
CD8+
C
P1
P2
CASP1
CASP5
CASP8
NLRP3
NLRP12
IL1A
IL1B
IL6
IL18
CXCL9
CXCL10
IFNG
IDO1
STAT1
STAT6
STAT2
STAT3
STAT4
STAT5B
JAK1
JAK2
JAK3
NFKB1
NFKB2
REL
RELA
RELB
NFKBIA
Inflammasome
IFN type II
JAK/STAT
NFκB
-2 -1 0 1 2
log2 fold change
D
SLC4A10
S100A8
MAFB
S100A9
CCL3L1
VCAN
SRP14
EGR1
SMAD7
NRCAM
CXCL8
G0S2
GABPB1-AS1
DUSP4
CD101
FCN1
C5AR1
THEMIS2
TAP2
TRIB1
TRGV5
APOBEC3A
CD300E
ADAM12
FCGBP
CADM1
OXNAD1
TRGC1
PLAUR
CXCL2
COL5A3
AC087741.1
NT5C
COLGALT2
LMNA
-log10 FDR
log2 fold change
E
IL-1β (pg/ml)
60
40
20
0

Fig 3

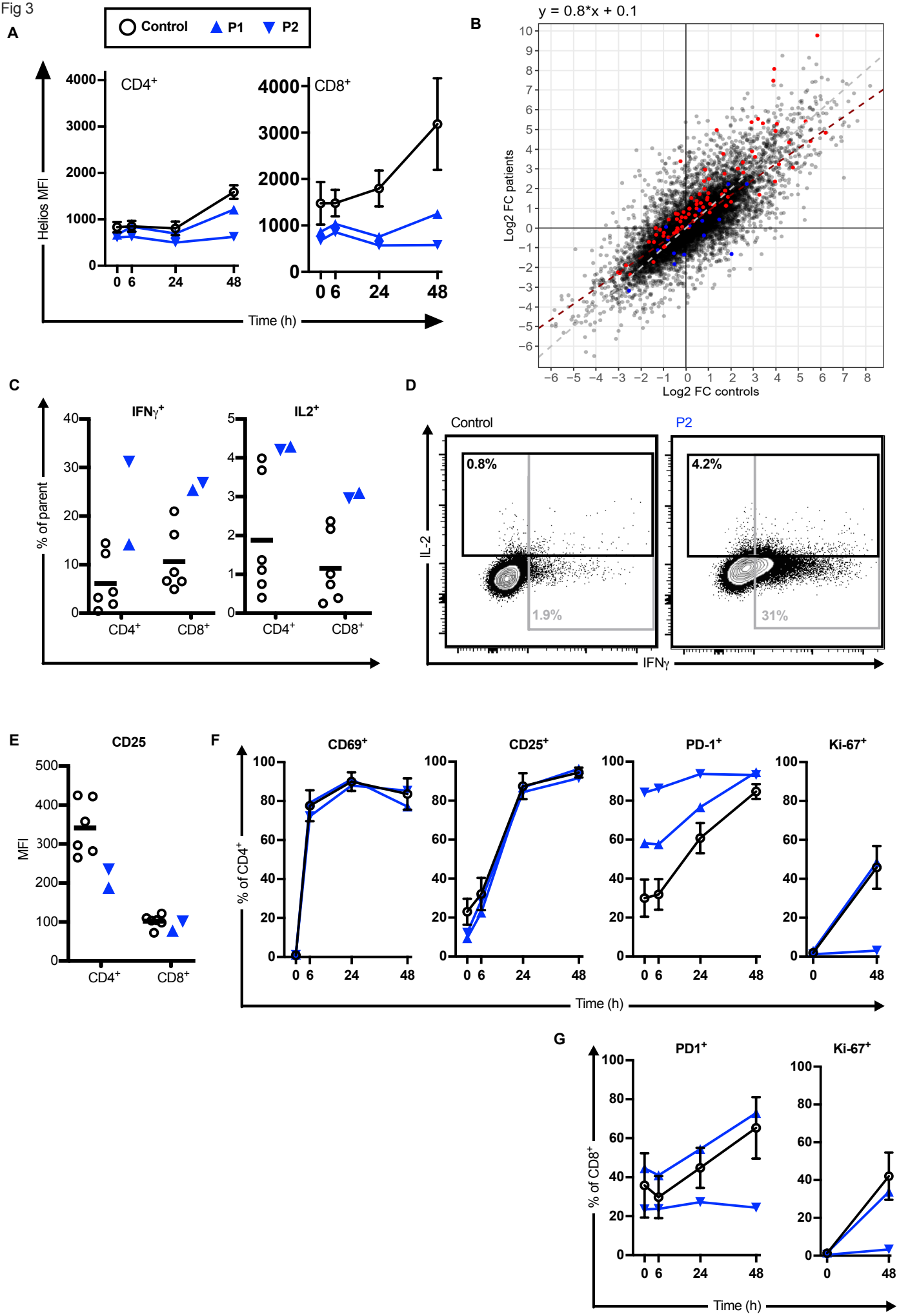
A
Control
P1
P2
CD4+
CD8+
Helios MFI
Time (h)
B
y = 0.8*x + 0.1
Log2 FC patients
Log2 FC controls
C
IFNγ+
IL2+
% of parent
CD4+
CD8+
D
Control
P2
0.8%
1.9%
4.2%
31%
IL-2
IFNγ
E
CD25
MFI
F
CD69+
CD25+
PD-1+
Ki-67+
% of CD4+
Time (h)
G
PD1+
Ki-67+
% of CD8+
Time (h)

Fig 4

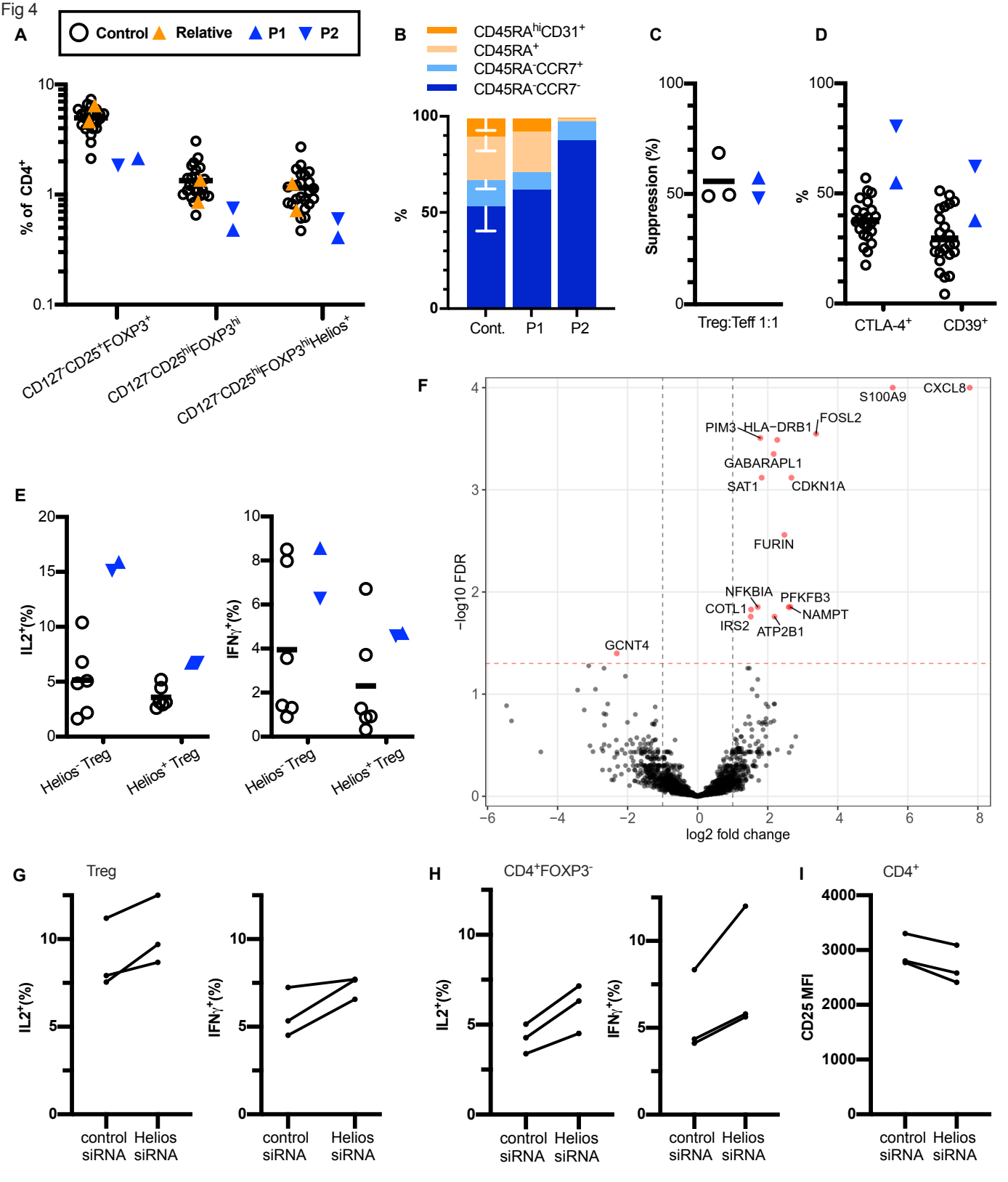
A
Control
Relative
P1
P2
% of CD4+
CD127-CD25+FOXP3+
CD127-CD25hiFOXP3hi
CD127-CD25hiFOXP3hiHelios+
B
CD45RAhiCD31+
CD45RA+
CD45RA-CCR7+
CD45RA-CCR7-
%
Cont.
P1
P2
C
Suppression (%)
Treg:Teff 1:1
D
%
CTLA-4+
CD39+
E
IL2+(%)
IFNγ+(%)
Helios- Treg
Helios+ Treg
F
−log10 FDR
log2 fold change
CXCL8
S100A9
FOSL2
PIM3
HLA-DRB1
GABARAPL1
SAT1
CDKN1A
FURIN
NFKBIA
PFKFB3
COTL1
NAMPT
IRS2
ATP2B1
GCNT4
G
Treg
IL2+(%)
IFNγ+(%)
control siRNA
Helios siRNA
H
CD4+FOXP3-
IL2+(%)
IFNγ+(%)
control siRNA
Helios siRNA
I
CD4+
CD25 MFI
control siRNA
Helios siRNA

Fig 5

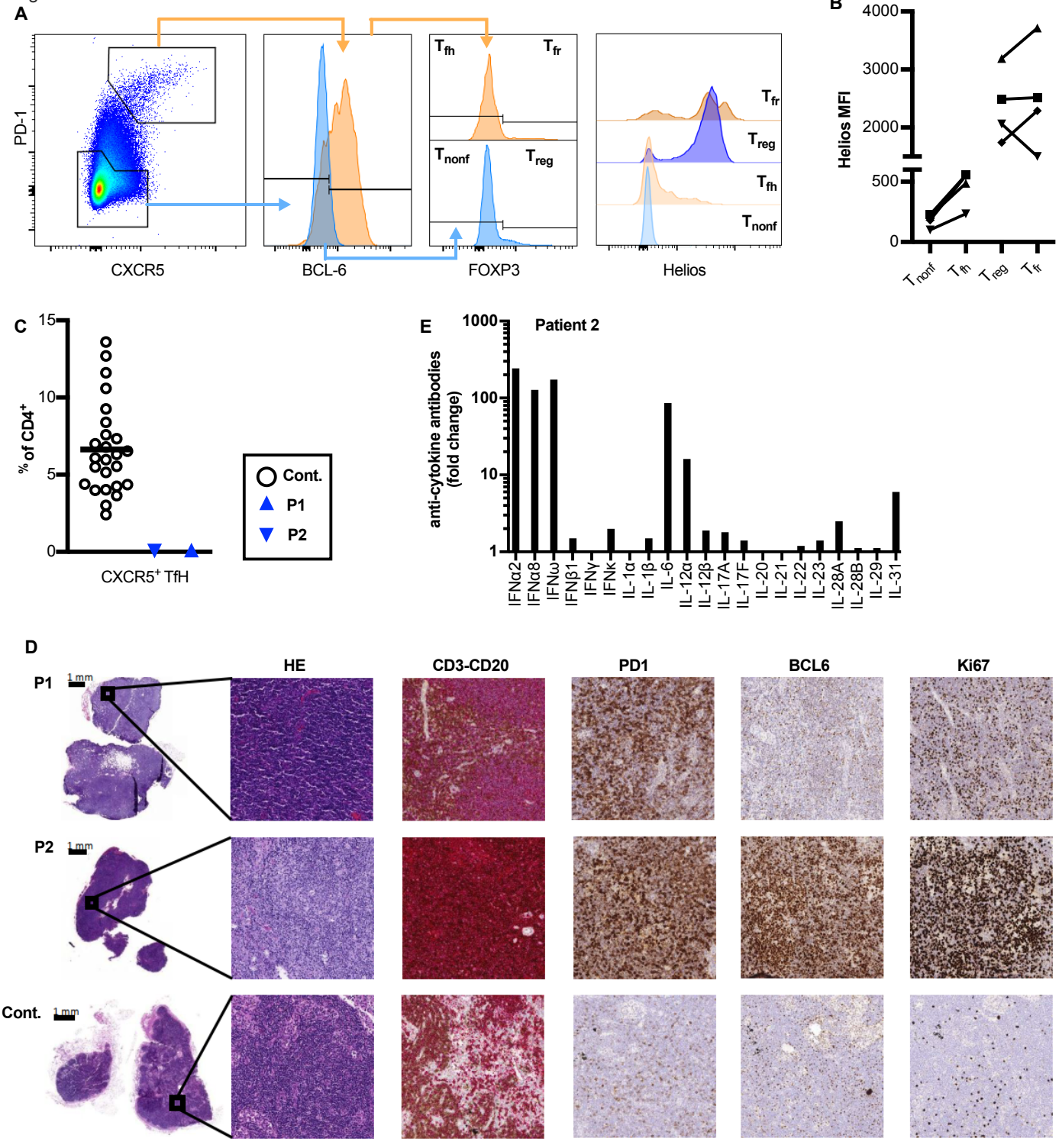
A
PD-1
CXCR5
BCL-6
T_{fh}
T_{fr}
T_{nonf}
T_{reg}
FOXP3
Helios
B
Helios MFI
4000
3000
2000
500
0
T_{nonf}
T_{fh}
T_{reg}
T_{fr}
C
% of CD4+
15
10
5
0
CXCR5+ TfH
Cont.
P1
P2
E
Patient 2
anti-cytokine antibodies (fold change)
1000
100
10
1
IFNα2
IFNα8
IFNω
IFNβ1
IFNγ
IFNκ
IL-1α
IL-1β
IL-6
IL-12α
IL-12β
IL-17A
IL-17F
IL-20
IL-21
IL-22
IL-23
IL-28A
IL-28B
IL-29
IL-31
D
HE
CD3-CD20
PD1
BCL6
Ki67
P1
P2
Cont.
1 mm

Fig 6

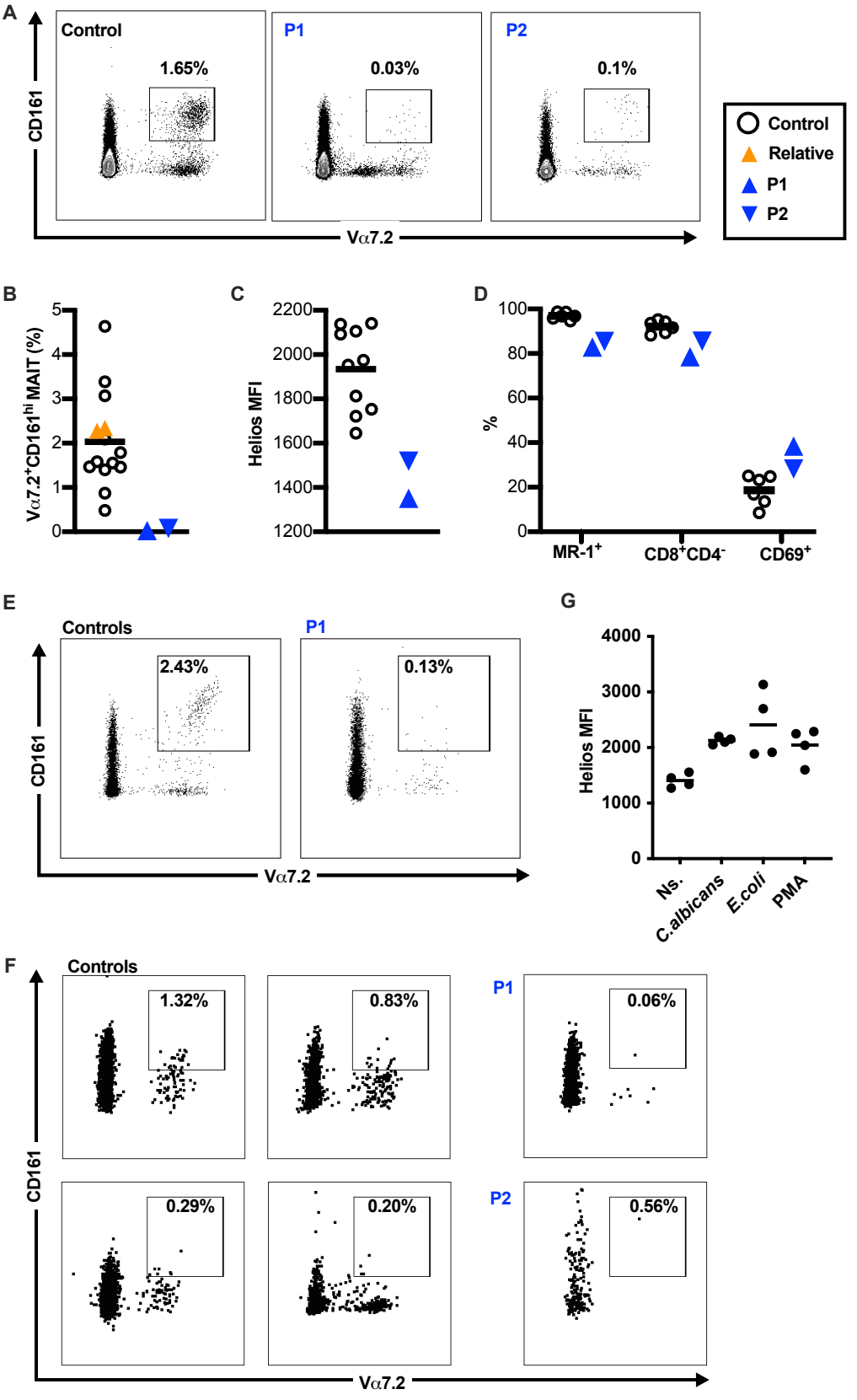
A
Control
1.65%
P1
0.03%
P2
0.1%
CD161
Vα7.2
Control
Relative
P1
P2
B
Vα7.2+CD161hi MAIT (%)
C
Helios MFI
D
%
MR-1+
CD8+CD4-
CD69+
E
Controls
2.43%
P1
0.13%
CD161
Vα7.2
G
Helios MFI
Ns.
C.albicans
E.coli
PMA
F
Controls
1.32%
0.83%
P1
0.06%
0.29%
0.20%
P2
0.56%
CD161
Vα7.2

Supplementary Clinical Data

Patient 1 is a woman that was admitted to immunodeficiency clinic at the age of 39. She has suffered from recurrent *Candida albicans* vulvovaginitis with painful genital ulcerations since the age of 30. The patient has had occasional aphthae also in her mouth and recurrent sinusitis. The diagnosis of common variable immunodeficiency was made when she was 39 years old and hypothyroidism diagnosis a year after that. The same year, some round, mildly enlarged lymph nodes were found in the right armpit and under the right pectoralis major muscle, histology showed cortical follicular hyperplasia. Immunoglobulin replacement therapy was started two years after the diagnosis: with a weekly dose of 30–40 ml the situation got significantly better and yeast infection relapses are now rare. After initiation of the immunoglobulin replacement therapy, she had a herpes zoster infection in the left chest area and she had two sinusitis with continuous sensation of nasal fullness. Weekly SCIG dose elevation to 60 ml did not help and antrostomy (FESS) on both sides was performed. While on SCIG, patient has been treated succesfully for *Helicobacter pylori*. Fecal parasites were examined due to persistent diarrhea and *Dientamoeba fragilis* was found and treated. Diarrhea persisted after succesfull eradication and a colonoscopy was made with normal macroscopic and histological findings.

Patient 2 is the father of Patient 1 and he was examined at the immunodeficiency clinic first time at the age of 63 years. During his working years, he had approximately two pneumonias yearly, after he has been examined for immunodeficiency he had one radiologically confirmed pneumonia two years ago. He has had a mild wound infection twice after surgery. Lichen planus of the upper extremities and gluteal area has reappeared over the years. At the age of 35, Morbus Hodgkin was diagnosed in a lymph node of the left armpit. The lymphoma was treated with splenectomy and radiation therapy that resulted in hypothyroidism and mild fibrosis of the lungs, for which he uses intermittent glucocorticoid inhalations and gets occasional oral candidiasis. 16 years later, an enlarged lymph node was removed from the right inguinal area, histology showed lymphatic hyperplasia. *Helicobacter pylori* has been cleared with antibiotics. The patient has always had loose stools several times a day, colonoscopy two years after diagnosis showed mild irritation of the ileum but histology was normal.

The mother of patient 2 was tested negative for IKZF2 mutation. The father of patient 2 had died several years prior and according to information given by patient 2 did not present with any signs of immune dysregulation.

Clinical findings

	patient 1	patient 2
Viral infections		
Aphtae	x	x
HSV	~	~
VZV (zoster)	x	I
HPV high risk	~	(-)
CMV	~	I
Bacterial infections		
Recurrent sinusitis	x	~
Recurrent pneumonia	~	x
Surgical wound infection	~	x
HePy	x	x
Yeast infections		
Mouth	~	x
Candida vaginitis	x	(-)
Parasitic infections		
Dientamoeba fragilis	x	~
Giardia	~	~
Autoimmunity		
Vitiligo	x	~
Lichen	~	x
Colitis	~	x
Hypothyreosis	x	x
Lymphatic tissue		
Follicular hyperplasia	x	x
Lymphoma	~	x
Splenectomy	~	x
Vaccine responses		
StPn polysaccharide	4/10	N
StPn conjugate	2/9	N
Menigococcus	(-)	N
Tetanus	low	N
Diphteria	low	N
Measles	low	I
Rubella	N	I
Parotitis	N	I
Hib	(-)	N
HBV	low	(-)
HAV	N	(-)
Other		
C3	1.47 low	1.36 / N
Monosytosis	N	0.81-0.92/12%
Interferon1 autoAb	N	elevated
Plasma IL2R	535 N	201 N

HSV - Herpes simplex virus, S- HSVAb neg and no symptoms
VZV - Varicella zoster virus, zoster symptoms and VZV-IgG pos (patient 1), no syptoms and VZV-IgG pos (patient 2)
HPV - Human papilloma virus, high risk subgroups, PCR from cervix
CMV - P-CMVNh neg Patient 1
HePy - Helicobacter pylori, fecal antigens
StPn - Streptococcus pneumoniae
Hib - Hemophilus influenzae
HBV - Hepatitis B virus
HAV - Hepatitis A virus

~ - negative findings
x - positive findings
(-) - not measured
N - normal findings
I - natural immunity: positive IgG, no IgM

Fig S1

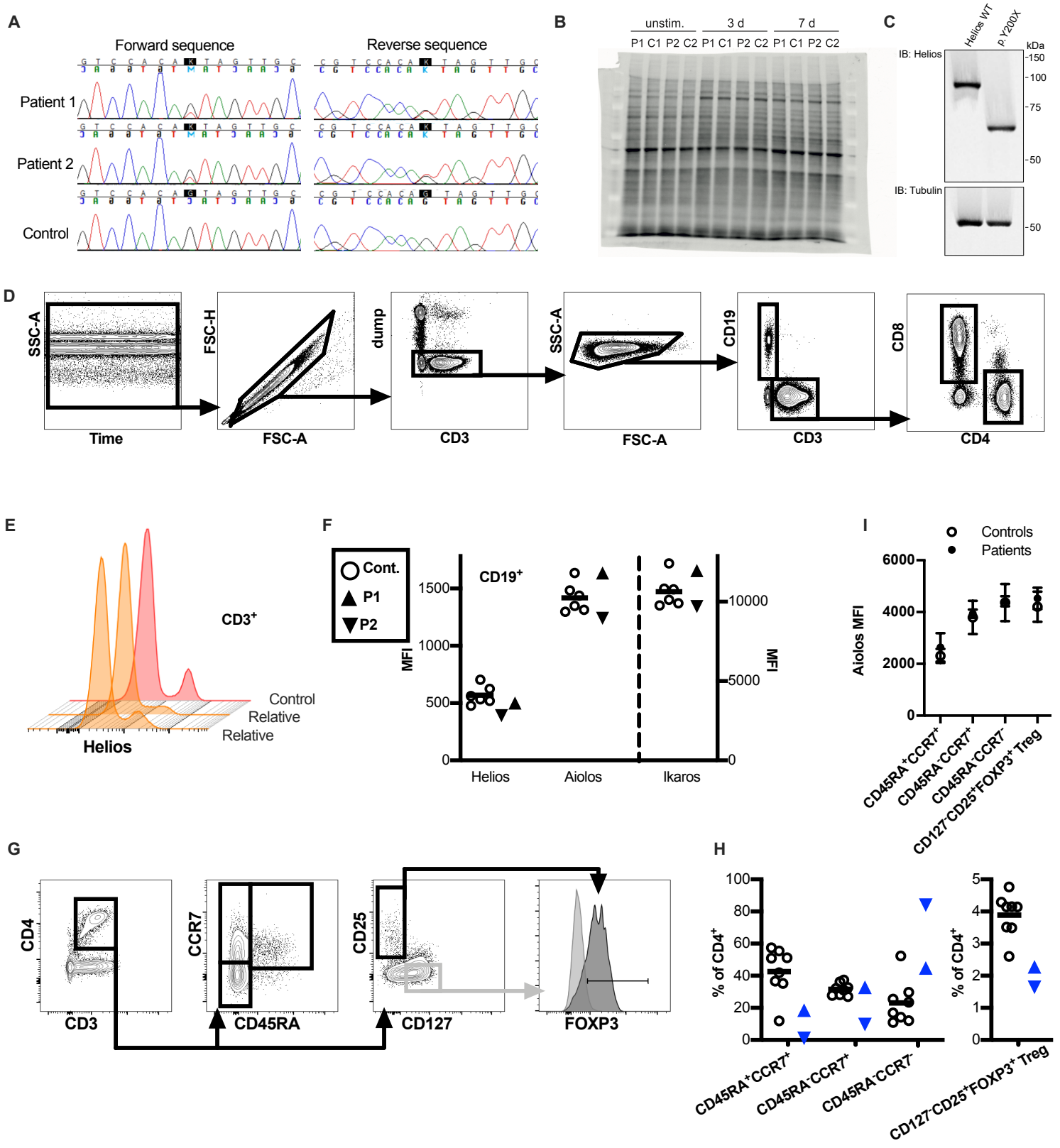

Figure S1: Targeted capillary sequencing of *IKZF2* and gating strategy to measure Ikaros family transcription factors
(A) Targeted capillary sequencing of cDNA derived from the RNA of patients and healthy control, respectively. (B) Total protein staining for the immunoblot shown in Fig 1B. (C) Anti-Helios antibody used in Fig 1B detects both recombinantly expressed wild type Helios and p.Y200X variant protein. (D) Gating strategy to identify B cells, CD4+ T cells and CD8+ T cells from peripheral blood to calculate mean fluorescence intensity for transcription factors Helios, Aiolos and Ikaros displayed in Figure 1C-D. CD19+CD3- B cells and CD19-CD3+ T cells were gated from live CD14- lymphocytes. CD4+CD8- and CD8+CD4- T cells were further identified from the T cell population. (E) Histogram showing Helios expression in two healthy relatives of patients and representative unrelated healthy control. (F) Mean fluorescence intensity (MFI) for Ikaros transcription factors in CD19+ B cells. Expression in CD4+ and CD8+ T cells is shown Fig 1C. (G) Gating strategy to evaluate Aiolos expression in different subpopulations of CD4+ cells, (H) frequency of these subpopulations and (I) Aiolos MFI in these subpopulations in patients compared to healthy controls (n=6). Cut-off for FOXP3+ positive cells was determined from FOXP3 expression of CD3+CD4+CD25-CD127+ T cells (light gray). Gating strategy is shown for healthy 39 years old male (D,G). P1=patient 1, P2=patient 2, (black triangles). Dump channel = dead cell marker and CD14.

Fig S2

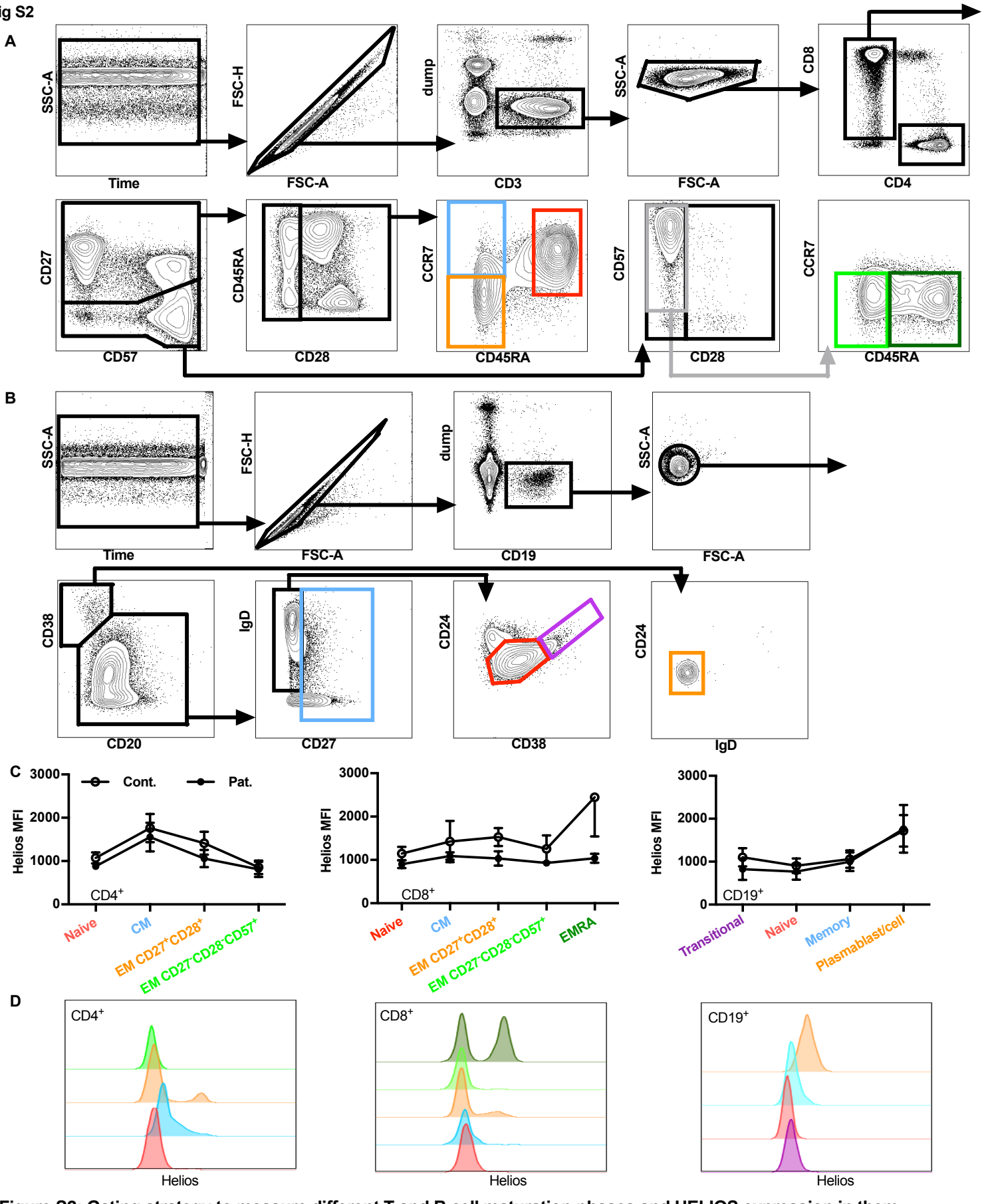

Figure S2: Gating strategy to measure different T and B cell maturation phases and HELIOS expression in them

(A) Gating strategy to identify T and B cell maturation phases from peripheral blood depicted in Figure 2A&B and to measure their HELIOS expression. CD4+CD8- and CD8+CD4- T cells were gated from live CD14-CD19-CD3+ cells. These populations were divided by the expression of CD27 and CD28. CD27+CD28+CCR7+CD45RAhi naive (red) CD27+CD28+CCR7+CD45RA- central memory (blue), CD27+CD28+CCR7-CD45RA- effector memory (orange), CD27-CD28-CCR7-CD45RA-CD57+ effector memory (light green) and CD27-CD28-CCR7-CD45RA+CD57+ effector memory RA+ (dark green) cells were identified. Gating strategy in CD8+ cells is shown for healthy 45 years old male. This gating strategy was also utilized to identify T cell populations depicted in Fig 2A&B. Dump = dead cell marked, CD19, CD14. (B) Cells of B cell lineage were identified as live CD3-CD14-CD19+cells. Transitional B cells were defined CD20+CD27-IgD+CD38hiCD24hi (violet), naive B cells CD20+CD27-IgD+CD38medCD24med (red) and memory B cells CD20+CD27- (blue). Plasma cells and -blasts were CD20-Cd38hiCD24-IgD- (orange). Gating strategy is shown for a healthy 38 years old female. Dump = dead cell marked, CD14, CD3. (C) Mean fluorescence intensity of HELIOS in respective lymphocyte populations in healthy controls (n=6) and patients. (D) Histograms depicting HELIOS expression in respective lymphocyte populations in representative healthy control.

Fig S3

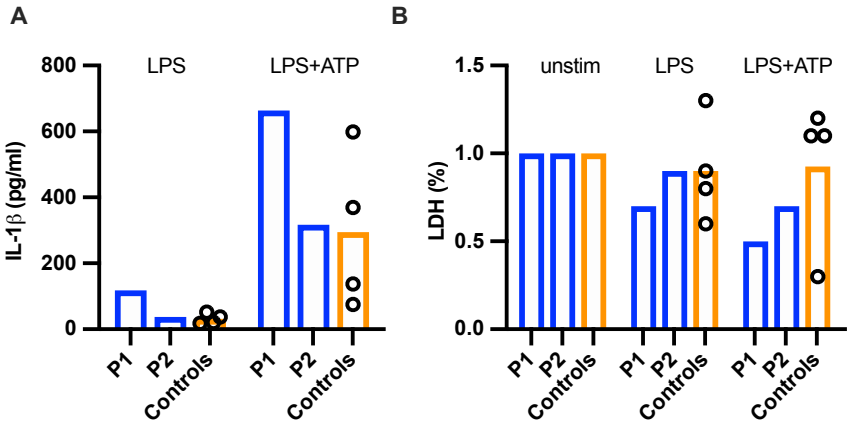

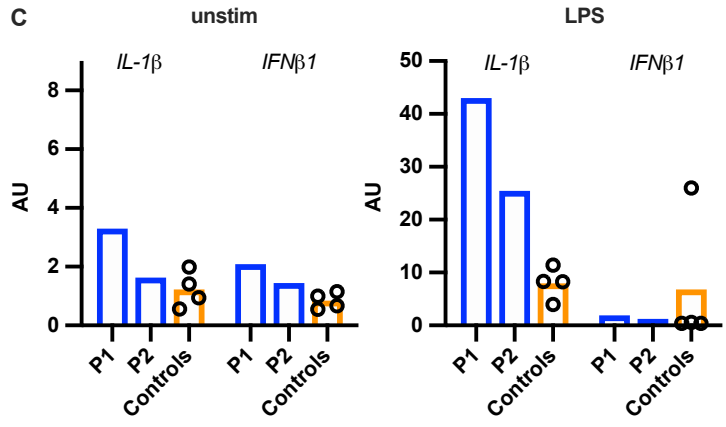

Figure S3: Inflammasome activation in patients with the *IKZF2* p.Y200X variant

(A) PBMC of patients and healthy controls (n=4) were stimulated with LPS or combination of LPS and ATP, and IL-1β and (B) lactate dehydrogenase (LDH) were measured from culture supernatants. (C) Expression of *IL1B* and *IFNB1* were measured by quantitative PCR from PBMC without or with LPS stimulation. P1=patient 1, P2=patient 2.

Fig S4

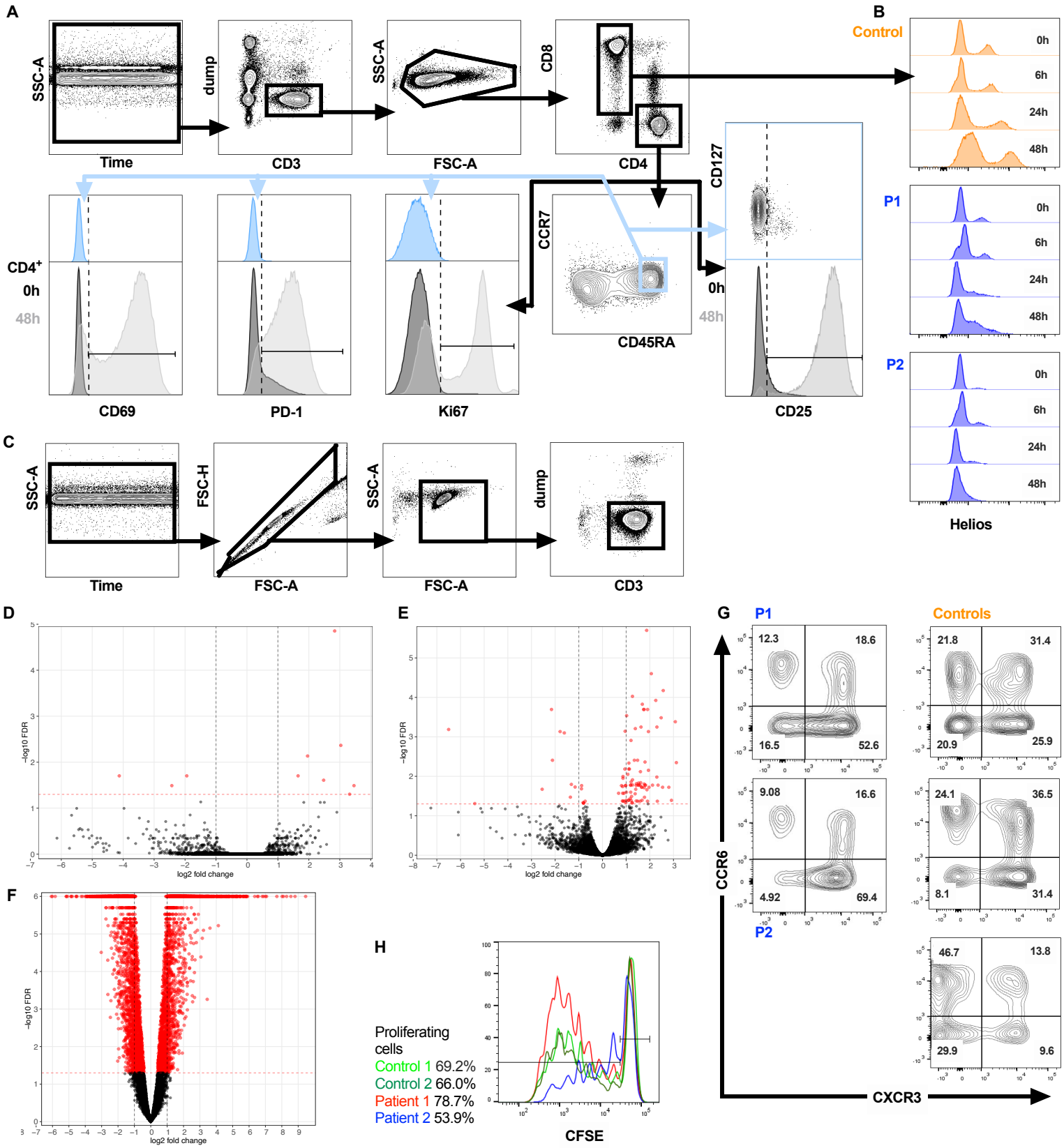

Figure S4: Gating strategy and volcano plots of T cell activation experiments

(A) Gating strategy to evaluate changes in activation markers after anti-CD3/CD28 stimulation. From live CD19-CD14-CD3+ lymphocytes with CD4+CD8- and CD4-CD8+ T cells were identified. Doublet discrimination was not performed as this would have resulted to unwanted exclusion of stimulated dividing cells. Expression of CD69, PD-1, Ki67 and CD25 was measured in different time points, here expression in CD4+CD8- cells ex vivo (black) and after 48h of stimulation (light gray) is shown in a representative control. Cut-off for positive cells was determined from expression of said markers in live CD19-CD14-CD3+CD4+CD8-CCR7+CD45RAhi naive T cells ex vivo (light blue). (B) Helios expression in CD8+ T cells in representative healthy control (orange), patient 1 and patient 2 (blue), respectively, in unstimulated sample and after 6, 24 and 48 hours of stimulation. (C) Additionally, the purity of CD3+ T cells was evaluated after bead purification. Gating strategy is shown with samples from a healthy 38 years old female (A, C). (D) Volcano plot of differentially expressed genes (red dots) in patients compared to healthy controls (n=5) in 3'RNA-seq data from purified CD3+ T cells without or (E) with anti-CD3-CD28 stimulation. (F) Volcano plot showing differentially expressed genes in anti-CD3-CD28 stimulated cells compared to unstimulated cells. (G) CCR6 and CXCR3 expression in CD4+CD45RA- memory helper T cells in patients 1 and 2 and healthy controls (n=3). Patients show a marked accumulation of CCR6-CXCR3+ Th1 cells in expense of other Th subsets, especially CCR6+CXCR3- Th17 cells. (H) CFSE staining of CD4+CD25-CD127+ effector T cells after 6 days of stimulation with anti-CD3/CD28 beads in patients 1 (red) and 2 (blue) and two healthy controls (light and dark green), respectively. Fraction of proliferating cells is shown. Dump = dead cell marked, CD19, CD14. P1=patient 1, P2=patient 2.

Fig S5

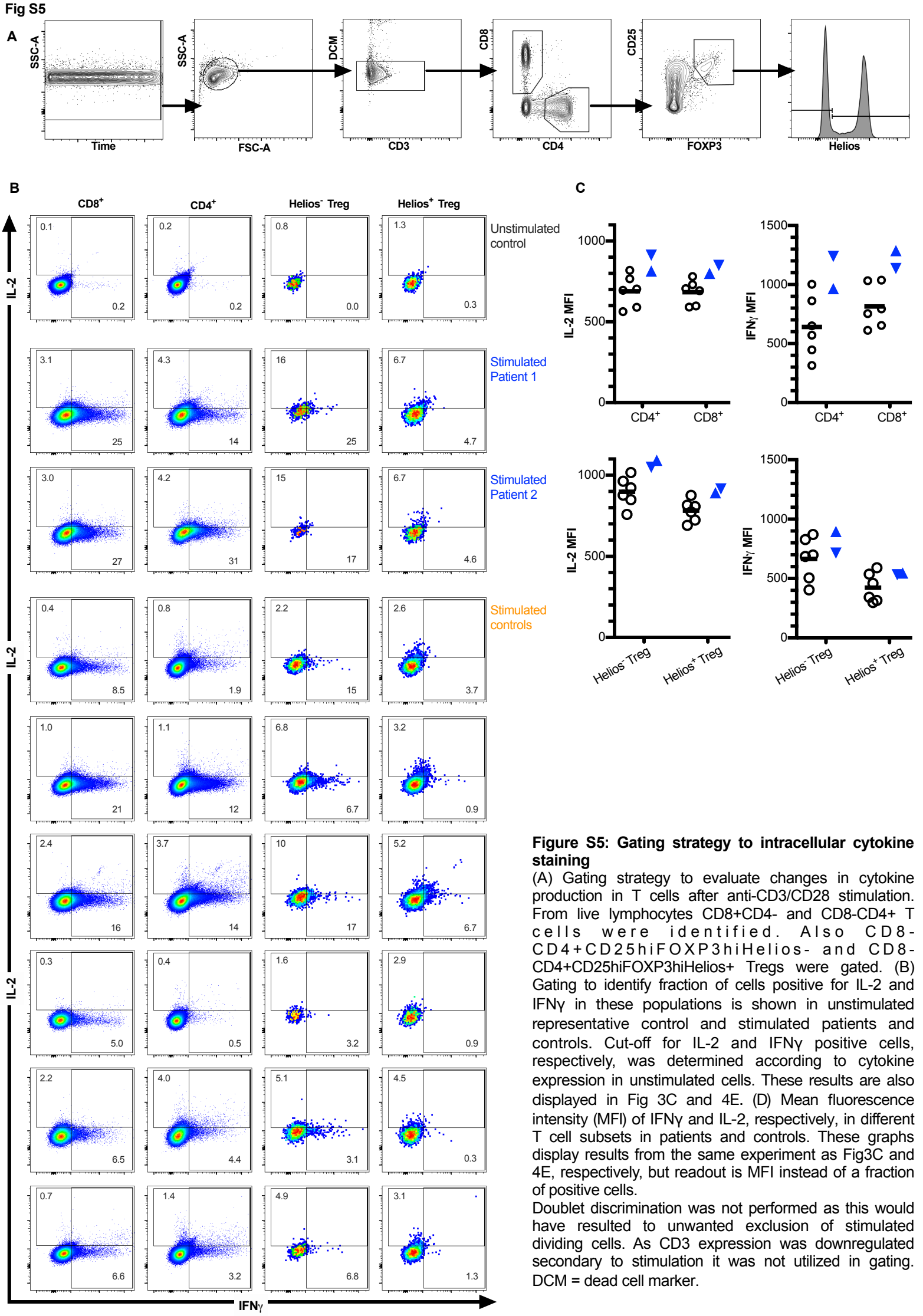

Figure S5: Gating strategy to intracellular cytokine staining

(A) Gating strategy to evaluate changes in cytokine production in T cells after anti-CD3/CD28 stimulation. From live lymphocytes CD8+CD4- and CD8-CD4+ T cells were identified. Also CD8-CD4+CD25hiFOXP3hiHelios- and CD8-CD4+CD25hiFOXP3hiHelios+ Tregs were gated. (B) Gating to identify fraction of cells positive for IL-2 and IFNγ in these populations is shown in unstimulated representative control and stimulated patients and controls. Cut-off for IL-2 and IFNγ positive cells, respectively, was determined according to cytokine expression in unstimulated cells. These results are also displayed in Fig 3C and 4E. (D) Mean fluorescence intensity (MFI) of IFNγ and IL-2, respectively, in different T cell subsets in patients and controls. These graphs display results from the same experiment as Fig3C and 4E, respectively, but readout is MFI instead of a fraction of positive cells.

Doublet discrimination was not performed as this would have resulted to unwanted exclusion of stimulated dividing cells. As CD3 expression was downregulated secondary to stimulation it was not utilized in gating. DCM = dead cell marker.

Fig S6

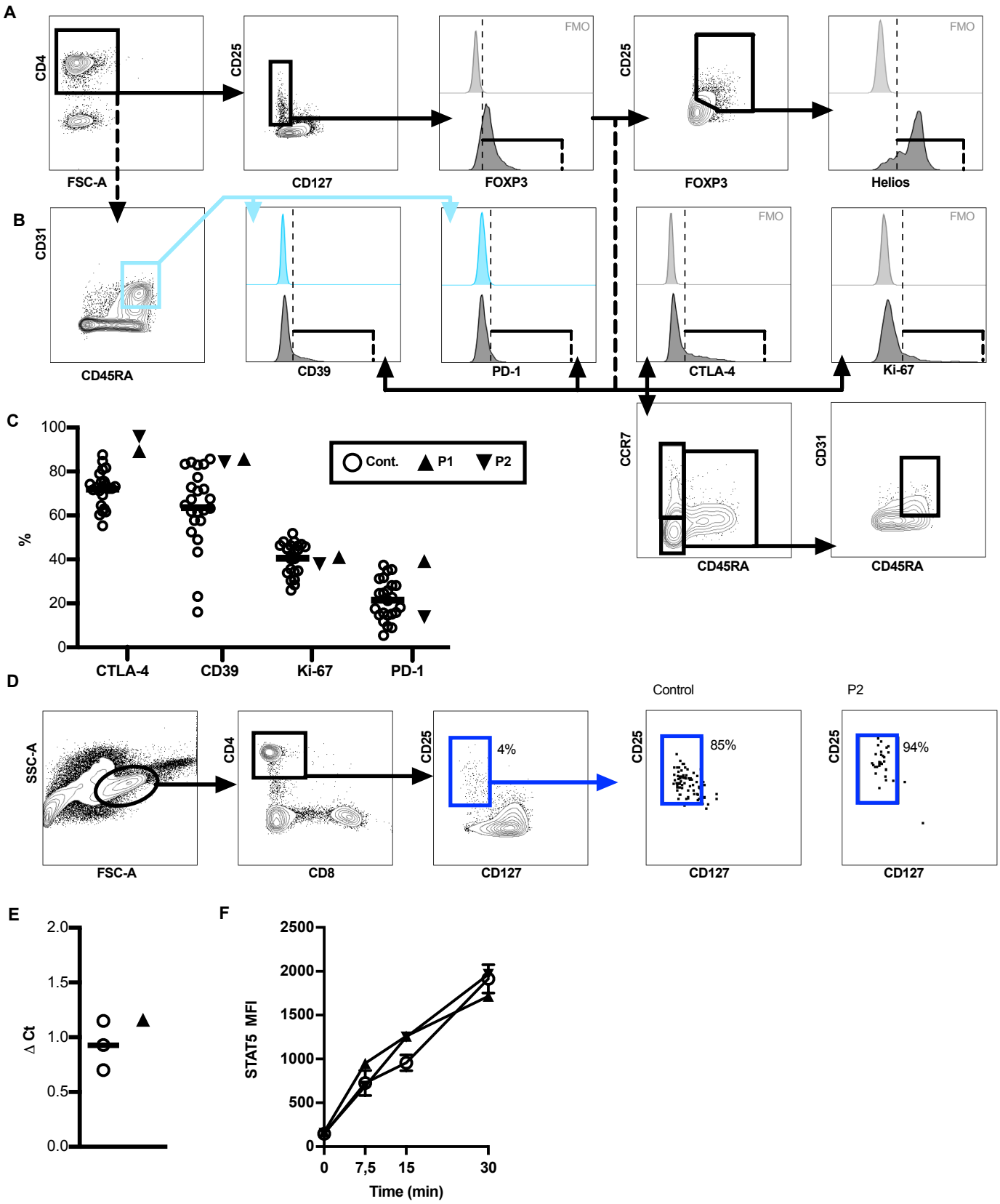

Figure S6: Gating strategy to regulatory T cell experiments

(A) Gating strategy to identify Tregs from peripheral blood. Live CD14-CD19-CD3+ T lymphocytes were gated as in Suppl Fig 2A. CD4+CD127-CD25+FOXP3+, CD4+CD127-CD25hiFOXP3hi and CD4+CD127-CD25hiFOXP3hiHelios+ Tregs were identified (displayed in Fig 4A). Cut-off for FOXP3 and Helios positive cells, respectively, was determined with the help of fluorescence minus one staining (FMO) (light gray). (B) In a different panel with same gating strategy live CD14-CD19-CD3+CD4+CD127-CD25+FOXP3+ Tregs were identified and their maturation phase was evaluated (displayed in Fig 4B). CD45RA+ cells shown in Fig 4B account for all the other CD45RA+ cells except CD45RAhiCD31+ cells and CCR7+CD45RA- and CCR7-CD45RA- were gated as shown above. Additionally, the proportion of Tregs cells expressing CTLA-4 and CD39 (displayed in Fig 4D), and, Ki67 and PD-1 was measured. Cut-off for CTLA-4 and Ki-67 positive cells, respectively, was determined with the help of FMO (light gray) and for CD39 and PD-1 positive cells, respectively, with the help of expression of said markers in CD4+CD45RAhiCD31hi cells recent thymic emigrant T cells (light blue). Gating strategy is shown for healthy 45 years old male (A&B). (C) Expression of different surface markers of CD4+CD127-CD25hiFOXP3hi Tregs in patients and controls. Gating for CTLA-4, Ki-67, CD39 and PD-1 was done as shown in B. (D) Sorting strategy to CD4+CD127-CD25hi Tregs and purity in representative healthy control and patient 2 (P2). (E) Degree of methylation in CD4+CD127-CD25hi Tregs in patient 1 and three healthy controls. The data are shown on a relative scale as change of Ct: ΔCt = Ct(demethylated DNA) - Ct(methylated DNA). (F) STAT5 MFI in response to IL-2 stimulation at different time points in patients and healthy controls (n=3). P1=patient 1, P2=patient 2.

Fig S7

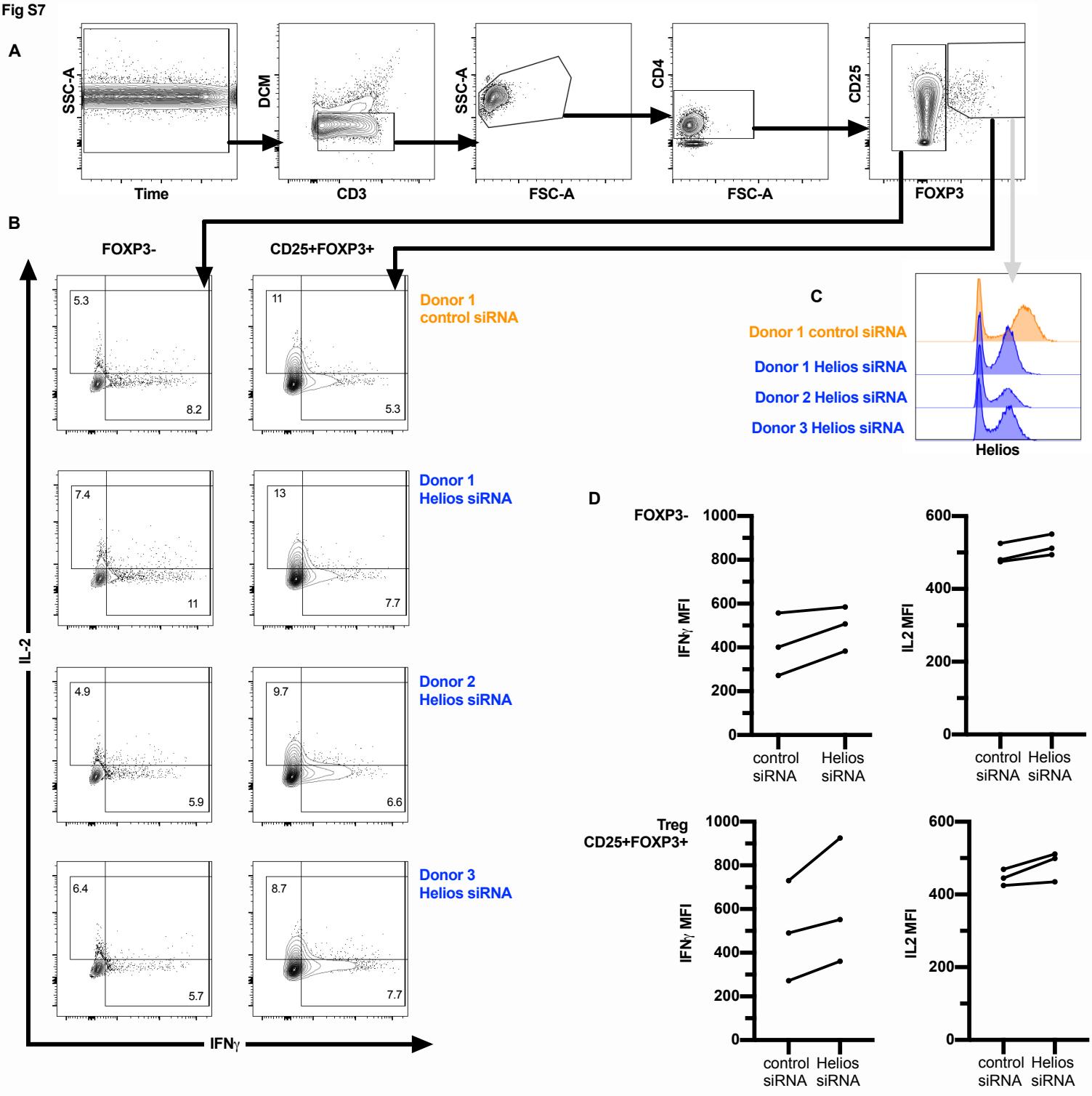

E

	Helios siRNA Log2 fold change compared to control siRNA			
	Donor 1	Donor 2	Donor 3	Donor 4
IKZF2	-0,83	-0,94	-0,87	-0,57

Figure S7: Gating strategy to siRNA experiment

(A) Gating strategy to evaluate changes in cytokine production of siRNA treated cells after 24 hour anti-CD3/CD28 stimulation and with Brefeldin A for the last 6 hours of incubation. From live lymphocytes CD3+CD4+ T cells FOXP3- T cells and CD25+FOXP3+ Tregs were identified. (B) Gating to identify fraction of cells positive for IL-2 and IFNγ in these populations is shown in control siRNA and Helios siRNA conditions, respectively, for subject 1 and in Helios siRNA condition for subjects 2 and 3. Cut-off for IL-2 and IFNγ positive cells, respectively, was determined according to cytokine expression of stimulated negative control siRNA treated cells. Results from all subjects are displayed in Fig 4 G-I. (C) Helios expression in stimulated live CD3+CD4+CD25+FOXP3+ Tregs in control siRNA and Helios siRNA conditions, respectively, for subject 1 and in Helios siRNA condition for subjects 2 and 3. (D) Mean fluorescence intensity (MFI) of IFNγ and IL-2, respectively, in CD3+CD4+ T cells FOXP3- T cells and CD25+FOXP3+ Tregs. These graphs display results from the same experiment as Fig4 G-H, but readout is MFI instead of a fraction of positive cells. (E) Log2 fold change of *IKZF2* expression in Helios siRNA treated cells compared to control siRNA treated cells (n=4) as measured by Nanostring. Only samples with over -0.8 log2 fold change reduction were qualified for further analysis (n=3).

Doublet discrimination was not performed as this would have resulted to unwanted exclusion of stimulated dividing cells. DCM = dead cell marked.

Fig S8

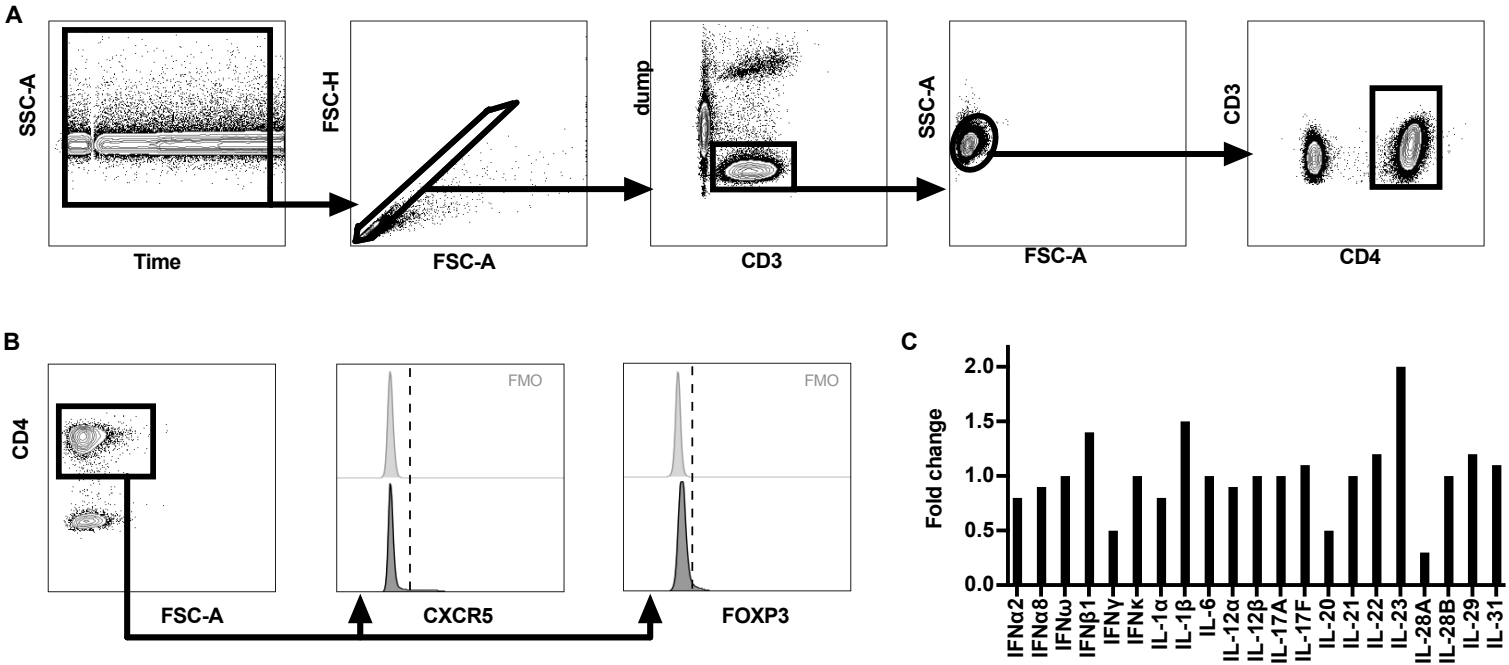

Figure S8: Gating strategy to follicular T helper cell quantification and auto-antibodies in patient 1
(A) Gating strategy to identify TfH cells from lymph nodes. Gating to identify CD14-CD19-CD3+CD4+ T lymphocytes is shown in 19 years old male. Rest of the gating strategy is shown in Fig 5A. (B) Gating strategy to identify TfH cells from peripheral blood. Live CD14-CD19-CD3+ T lymphocytes were gated as in Suppl Fig 2A. CD4+ cells expressing CXCR5 and FOXP3 were identified from them with help of fluorescence minus one stainings (FMO; gray). Gating strategy is shown for healthy 45 years old male. (C) Auto-antibodies against cytokines in patient 1. Fold change compared to the mean of healthy controls (n=5) is shown.

Fig S9

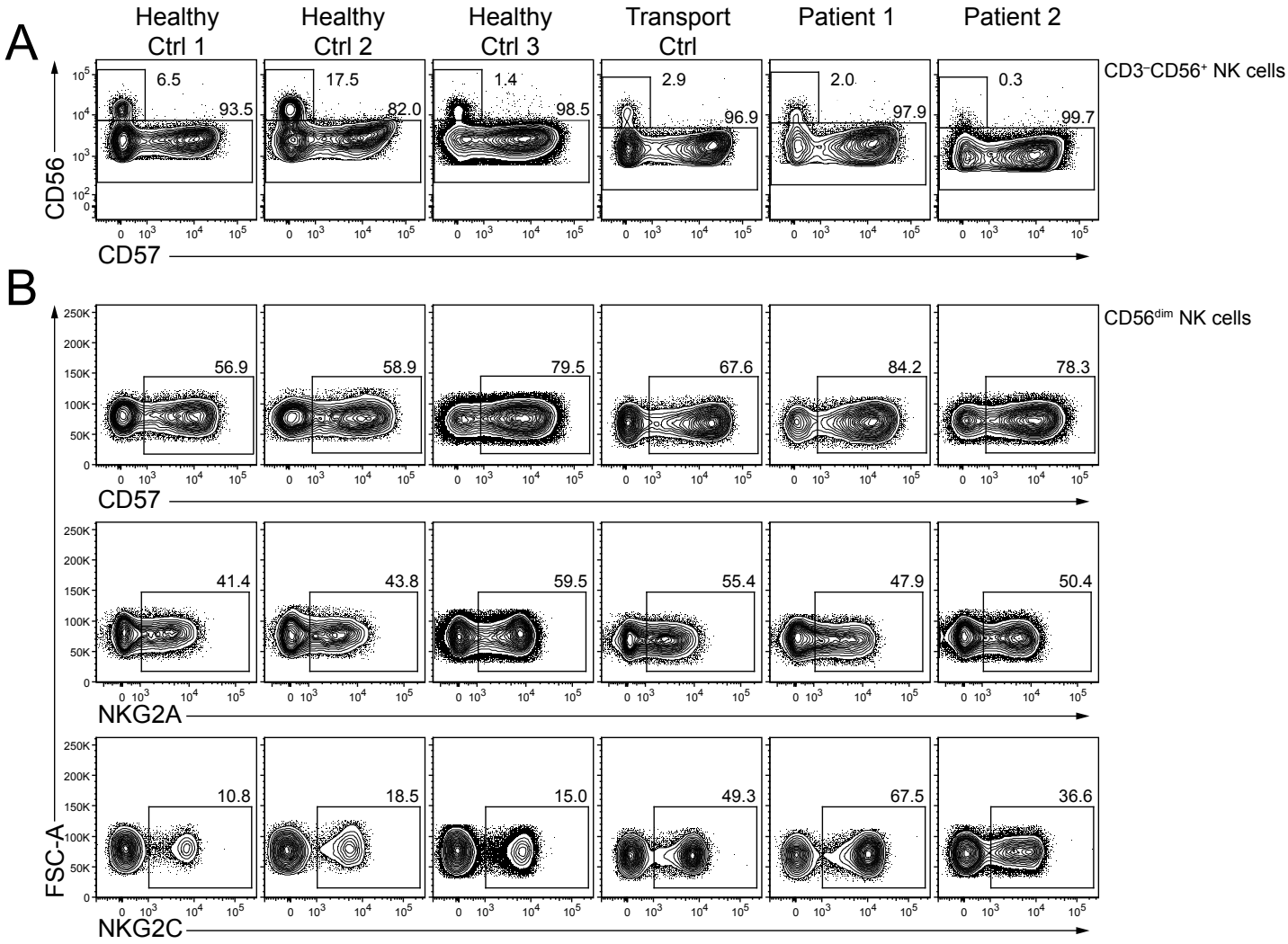

Figure S9: NK cell phenotype in patients with the *IKZF2* p.Y200X variant
(A) Proportions of CD56brightCD16- and CD56dimCD16+ NK cells in controls and patients, (B) Proportions of fully mature CD57+, naïve NKG2A+, and adaptive-like NKG2C+ CD56dim NK cells in patients and controls.

Fig S10

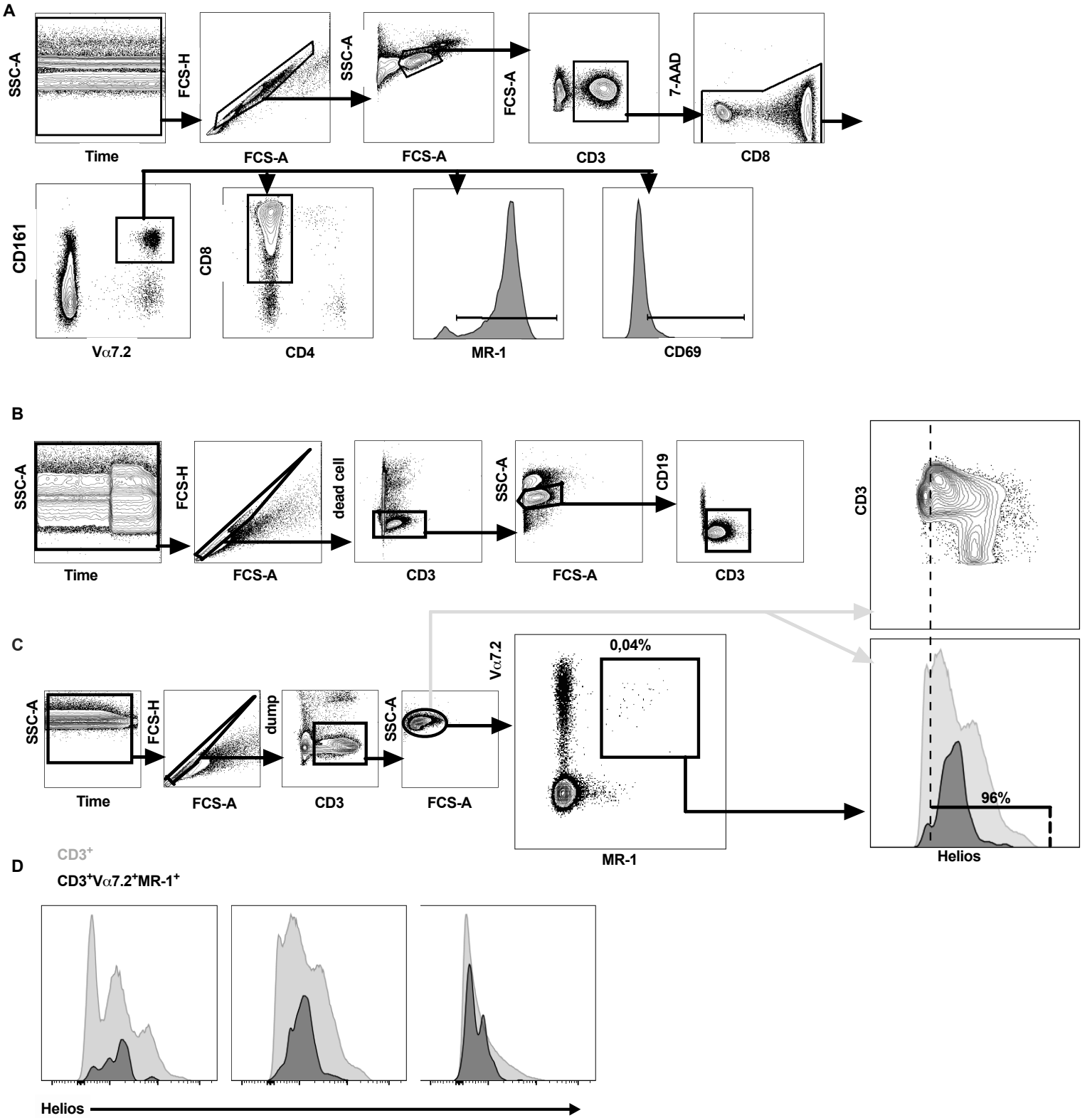

Figure S10: Gating strategy to MAIT experiments

(A) Functional characteristics of MAITs were analyzed from freshly isolated PBMCs. From live CD3+Vα7.2+CD161+ MAITs expression of MR-1 and CD69 and the proportion of CD8+CD4- cells were evaluated (displayed in Fig 6D). (B) From duodenum and colon live CD19-CD3+ were first gated and MAITs identified as Vα7.2+CD161hi cells as shown in Fig 6 D&E. (C) Developing MAITs were identified from thymus as live CD19-CD14-CD3+Vα7.2+MR-1+ thymocytes. Cut-off for HELIOS positive cells was determined from Helios expression of all live CD3+ thymocytes (light gray). (D) Histograms showing Helios expression in all CD3+ thymocytes (light gray) and CD3+Vα7.2+MR-1+ thymocytes (black). Gating strategy is shown with PBMC from a healthy 44-year-old female (A) with a thymic sample from a 15 days old male (B) and duodenal sample from a 34-year-old female (D). Gating to identify live CD19-CD14-CD3+ T cells from peripheral blood to gate MAITs in Fig 6A-C was done as in Fig S2A.
Dump = dead cell marker, CD19 and CD14.